Signatures of extra dimensions in gravitational waves from black hole quasinormal modes

Sumanta Chakraborty,[1,*] Kabir Chakravarti,[2,†] Sukanta Bose,[2,3,‡] and Soumitra SenGupta[1,§]

[1]*Theoretical Physics Department, Indian Association for the Cultivation of Science, Kolkata 700032, India*
[2]*IUCAA, Ganeshkhind, Post Bag 4, Pune University Campus, Pune 411007, India*
[3]*Department of Physics and Astronomy, Washington State University, 1245 Webster, Pullman, Washington 99164-2814, USA*

(Received 30 October 2017; published 29 May 2018)

In this work, we have derived the evolution equation for gravitational perturbation in four-dimensional spacetime in the presence of a spatial extra dimension. The evolution equation is derived by perturbing the *effective* gravitational field equations on the four-dimensional spacetime, which inherits nontrivial higher-dimensional effects. Note that this is different from the perturbation of the five-dimensional gravitational field equations that exist in the literature and possess quantitatively new features. The gravitational perturbation has further been decomposed into a purely four-dimensional part and another piece that depends on extra dimensions. The four-dimensional gravitational perturbation now admits massive propagating degrees of freedom, owing to the existence of higher dimensions. We have also studied the influence of these massive propagating modes on the quasinormal mode frequencies, signaling the higher-dimensional nature of the spacetime, and have contrasted these massive modes with the massless modes in general relativity. Surprisingly, it turns out that the massive modes experience damping much smaller than that of the massless modes in general relativity and may even *dominate* over and above the general relativity contribution if one observes the ringdown phase of a black hole merger event at sufficiently late times. Furthermore, the whole analytical framework has been supplemented by the fully numerical Cauchy evolution problem, as well. In this context, we have shown that, except for minute details, the overall features of the gravitational perturbations are captured both in the Cauchy evolution as well as in the analysis of quasinormal modes. The implications on observations of black holes with LIGO and proposed space missions such as LISA are also discussed.

DOI: 10.1103/PhysRevD.97.104053

I. INTRODUCTION

Unification of forces has been the most challenging task the science community has ever faced. So far, that quest has successfully brought the electromagnetic, strong, and weak forces under one roof. However, the unification scheme hits a wall when one tries to incorporate in it the only other fundamental force, namely, gravity. There have been numerous attempts, so far, to incorporate gravity in the above picture, as well, leading to a unified quantum theory of nature. This has resulted in a large number of candidate theories for quantum gravity *but* without much success. This issue, broadly speaking, originates from the peculiar fact that the energy scale associated with grand unified theories is $\sim\mathcal{O}(10^3)$ GeV, whereas the natural energy scale for gravity is the Planck scale $\sim\mathcal{O}(10^{18})$ GeV. This huge difference between the respective energy scales manifests itself into unnatural fine tunings in various physical parameters of the model, e.g., in the mass of the Higgs Boson. Thus, it seems legitimate to understand the origin of this fine tuning problem (known as the gauge hierarchy problem) before delving into quantization of gravity [1–7].

One such natural candidate for resolving the gauge hierarchy problem in this regard corresponds to extra spatial dimensions, which can bring down the Planck scale to the realm of grand unified theories. Such a possibility was considered in [8–12], where the extra dimensions were large enough, such that the volume spanned by them could suppress the Planck scale of the higher-dimensional spacetime (known as *bulk*) to the TeV scale. However, this proposal harbors two conceptual drawbacks: First, it seems that the problem of energy scale hierarchy has merely been transferred to another form, the volume hierarchy; e.g., if one wants to reduce the energy scale to 1 TeV, the size of the extra dimensions would be $\sim 10^{11}$ m, and more importantly, it causes the higher-dimensional spacetime to be flat [1]. The second one is indeed a serious issue, as gravity

*sumantac.physics@gmail.com
†kabir@iucaa.in
‡sukanta@iucaa.in
§tpssg@iacs.res.in

cannot be shielded, and hence, if it is present in four dimensions, gravity is bound to propagate in higher spacetime dimensions, as well. In order to cure this problem, Randall and Sundrum proposed a very natural solution to the hierarchy problem with warped extra dimensions, where the presence of gravity in higher dimensions forces the effective Planck scale to reduce to TeV scale in the four-dimensional hypersurface we live in (known as *brane*) [13,14]. This scenario has been extensively studied in the literature in the past years in various contexts, starting from black holes [15–22] and cosmology [23–32] to particle phenomenology as well as possible signatures in Large Hadron Collider (LHC) [33–35]. Much attention has also been devoted to the higher curvature generalization of this scenario, obtained by introducing terms like R^2, $R_{abcd}R^{abcd}$ in the gravitational action, as well as to the stabilization of these extra dimensions [23,36–40].

Even though LHC provides us an observational window for the existence of extra spatial dimensions, it is important to know if there exists any other observational tests that can either prove or disprove their existence independently. It is obvious that in order to probe these effects, one has to investigate the high-energy/high-curvature regime, which can originate from either high-energy collisions such as in LHC or physics near black holes. The second possibility opens up a few interesting observational avenues: (a) the black hole continuum spectrum, originating from accretion disc around a supermassive black hole, (b) strong gravitational lensing around supermassive black holes, and finally, (c) gravitational waves from the collision of two massive black holes. We have already elaborated on the continuum spectrum from supermassive black holes and their implications regarding the presence of extra dimensions in [41], whereas strong gravitational lensing has been discussed in detail in [42]. In this work, we aim to address the third possibility, i.e., the effect of higher dimensions on gravitational waves, in light of the recent detections [43–47] of the same in Advanced Laser Interferometer Gravitational-Wave Observatory (aLIGO). The whole process of collision between two black holes can broadly be divided into three categories: inspiral phase, merger phase, and ringdown phase. The first two phases are best described by a combination of post-Newtonian and numerical approaches [48–63], which we leave for the future, concentrating here on the ringdown phase only. In this situation, the quasinormal mode frequencies play a very fundamental role in determining the ringdown phase, and in this work, we will concentrate on deriving the quasinormal mode frequencies for this higher-dimensional scenario [16,19,64–67].

To understand the behavior of quasinormal mode frequencies in the context of higher spacetime dimensions, one can follow two possible approaches. (a) One starts from the gravitational field equations in the bulk and then considers its perturbation around a bulk solution, which manifests itself as a black hole on the brane. This one we refer to as the *bulk-based approach*. (b) Otherwise, one projects the bulk gravitational field equations on the brane hypersurface, resulting in an effective description of the brane dynamics inherited from the bulk, referred to as the *brane-based approach*. In this case, as well, one perturbs the effective gravitational field equations on the brane, around a given bulk solution representing again a brane black hole. Some aspects of this problem along the first line of attack have already been elaborated and explored in [68–74]; however, to our knowledge, the second avenue is hitherto unexplored. In this work, we wish to fill this gap by providing a thorough analysis of the second approach in relation to the black hole perturbation theory and possible discords with the bulk-based approach. In particular, we will try to understand whether the results derived in [68] using Cauchy evolution of initial data matches with our quasinormal mode frequency analysis. Further for completeness, we will present the Cauchy evolution for the brane-based approach, as well. This will not only help to contrast these two approaches but also will depict whether the quasinormal mode analysis and the Cauchy evolution are compatible with each other. Besides providing yet another independent route towards understandings of higher dimensions, this will also be of significant interest to the gravitational wave community.

The paper is organized as follows: We start in Sec. II with a brief introduction of the effective equation formalism in the context of higher spatial dimensions, and then we build up our gravitational perturbation equation based on the above. This has been applied in Sec. III to derive the evolution equations for the master variables associated with spherically symmetric brane and possible effects from higher dimensions. In Sec. IV, we have studied these perturbation equations in Fourier space and have derived the quasinormal mode frequencies using the continued fraction method as well as the direct integration scheme. Using these quasinormal mode frequencies, the time evolution of the master variable has been determined for both the bulk- and the brane-based approach in Sec. V. Section VI deals with Cauchy evolution of the initial data and its possible harmony with the quasinormal mode analysis. We conclude with a discussion and implications of the results obtained in Sec. VII. Some detailed calculations pertaining to derivation of gravitational perturbation equation on the brane have been presented in Appendix A, and those associated with continued fraction method have been elaborated in Appendix B.

Note that we will set the fundamental constant c as well as the combination GM to unity, where M is the mass of the black hole. Indices running over all the bulk coordinates are denoted by uppercase Latin letters, and all the brane indices are denoted by Greek letters. Any geometrical quantity associated with the brane hypersurface alone is being denoted with a superscript (4). Further, all the matrix valued quantities will be denoted by boldfaced letters. Finally, the signature convention adopted in this work is the mostly positive one.

II. PERTURBING EFFECTIVE GRAVITATIONAL FIELD EQUATIONS ON THE BRANE

We start this section by providing a very brief introduction to the effective gravitational field equations on the brane, which will be necessary for our later purposes. Because we are interested in signatures of higher dimensions only, it will be sufficient to work within the context of Einstein gravity in five spacetime dimensions, in which case the gravitational Lagrangian density is the five-dimensional Ricci scalar R. Thus, the five-dimensional gravitational field equations will read $G_{AB} = 8\pi G_{(5)} T_{AB}$, where T_{AB} stands for the matter energy momentum tensor, which may be present in the bulk, and $G_{(5)}$ is the five-dimensional gravitational constant. In the specific context when the bulk energy momentum tensor originates from a negative cosmological constant Λ, one arrives at the following static and spherically symmetric solution on the brane:

$$ds^2_{\text{unperturbed}} = e^{-2ky}\left(-f(r)dt^2 + \frac{dr^2}{f(r)} + r^2 d\Omega^2\right) + dy^2, \tag{1}$$

with $f(r) = 1 - (2/r)$ and $k \propto \sqrt{-\Lambda}$. Note that from the perspective of a brane observer located on a $y =$ constant hypersurface, the spacetime structure on the brane is given by the Schwarzschild solution.

This raises the following interesting question: What happens to the gravitational field equations on the brane, given the gravitational field equations on the bulk? It has been answered for Einstein gravity in [75] and has been extended recently to various other scenarios involving alternative gravity theories [76–78]. The derivation goes as follows, one first chooses the brane hypersurface, say $y = 0$, and determines the normal $n_A = \nabla_A y$, yielding the induced metric on the brane hypersurface to be $h_{AB} = g_{AB} - n_A n_B$, such that $n_A h^A_B = 0$. Given the induced metric, one can introduce the notion of covariant derivative on a brane hypersurface and hence a notion of brane curvature using commutator between the brane covariant derivatives. This enables one to express the bulk curvature in terms of the brane curvature and extrinsic curvatures associated with the brane hypersurface. Further contractions will enable one to relate the bulk Einstein's equations with curvatures on the brane, referred to as the effective gravitational field equations on the brane. The effective equations in vacuum brane differ from four-dimensional Einstein's equations by an additional term inherited from the bulk Weyl tensor and takes the following form:

$$^{(4)}G_{\mu\nu} + E_{\mu\nu} = 0. \tag{2}$$

Here, $E_{\mu\nu}$ stands for a particular projection of the bulk Weyl tensor C_{ABCD} on the brane hypersurface (commonly known as the electric part) given by

$$E_{\mu\nu} = C_{ABCD} e^A_\mu n^B e^C_\nu n^D, \tag{3}$$

where n_A is the normalized normal introduced earlier and $e^A_\mu = \partial x^A / \partial y^\mu$ is the bulk to brane projector, with x^A being the bulk coordinates and y^μ the brane coordinates [79,80].

At this stage, it is worth mentioning that in order to arrive at the above relation we have assumed that the bulk cosmological constant and the brane tension cancels each other, leading to a vanishing effective cosmological constant on the brane hypersurface [13,75]. The above cancellation has its origin in the fact that in the effective field equation the effective cosmological constant is the difference between bulk cosmological constant and brane tension, and this difference has to be zero for the stability of the background spacetime. Further, note that even though Eq. (2) acts as the effective field equations on the brane, to solve it explicitly, one does require information of the bulk, hidden in $E_{\mu\nu}$ through the bulk Weyl tensor.

There are two ways to solve this equation: (a) Assume certain bulk geometry as ansatz [which for our case corresponds to Eq. (1)] and then try to see what sort of brane configuration solves Eq. (2). (b) Take $E_{\mu\nu}$ as an arbitrary tensor, and try to solve Eq. (2) with $E_{\mu\nu}$ treated as a source; e.g., in the context of spherical symmetry, one often divides $E_{\mu\nu}$ into an energy density (known as *dark radiation*) and pressure (known as *dark pressure*). Even though one can have very interesting results emerging from the second scenario [81], it has the drawback that the bulk metric remains unknown, and in general, it is not even clear whether there exists a bulk metric that would satisfy Einstein's equations in the bulk. Thus, we will adopt the first scenario and shall take Eq. (1) as the background metric which indeed satisfies (2), as well [76,81–84].

This procedure must be contrasted with the perturbation of bulk Einstein's equations around the solution presented in Eq. (1) because, in the case of effective field equations, the perturbation of the bulk Weyl tensor will play a crucial role. Thus, it is not at all clear *a priori* how the perturbed equations in the brane-based approach will behave in contrast to those in the bulk-based approach, even though they are being perturbed around the same solution. With this motivation in the backdrop, let us concentrate on perturbation of Eq. (3) around the bulk metric g_{AB} given in Eq. (1), such that

$$g_{AB} \to g_{AB} + h_{AB}. \tag{4}$$

Here, h_{AB} is the perturbed metric around g_{AB}, and all the expressions to follow will be evaluated to the first order in the perturbed metric h_{AB}.[1]

[1]In principle, one should write down $g_{AB} \to g_{AB} + \epsilon h_{AB}$, with small ϵ and then keep only terms linear in ϵ.

It is also well known that not all of the components of h_{AB} are dynamical; there are redundant gauge degrees of freedom. These gauge choices must be made according to convenience of calculations. In this particular situation, the following gauge conditions will turn out to be useful later:

$$\nabla_A h^A_B = 0; \qquad h^A_A = 0; \qquad h_{AB} = h_{\alpha\beta} e^\alpha_A e^\beta_B, \tag{5}$$

which is known as the Randall-Sundrum gauge. The usefulness of this gauge condition can also be anticipated from the fact that these imply $h_{AB}n^A = 0$, and hence the perturbed bulk metric takes the following form,

$$ds^2_{\text{perturbed}} = [q_{\alpha\beta}(y, x^\mu) + h_{\alpha\beta}(y, x^\mu)]dx^\alpha dx^\beta + dy^2, \tag{6}$$

where $q_{\alpha\beta}$ solves Eq. (2) and is given by

$$q_{\alpha\beta}dx^\alpha dx^\beta = e^{-2ky}\left(-f(r)dt^2 + \frac{dr^2}{f(r)} + r^2 d\theta^2 + r^2 \sin^2\theta d\phi^2\right). \tag{7}$$

Even though Eq. (1) opts for $f(r) = 1 - (2/r)$, in the rest of the analysis, we will keep $f(r)$ as general as possible. Then to linear order in the perturbed metric $h_{\alpha\beta}$, one can expand the four-dimensional Einstein tensor as

$${}^{(4)}G_{\mu\nu} \simeq {}^{(4)}G^{(q)}_{\mu\nu} + {}^{(4)}R^{(h)}_{\mu\nu} - \frac{1}{2}q_{\mu\nu}\,{}^{(4)}R^{(h)} - \frac{1}{2}h_{\mu\nu}\,{}^{(4)}R^{(q)}, \tag{8}$$

where terms with superscript (q) indicate that they have to be evaluated for the brane background metric $q_{\alpha\beta}$ given in Eq. (7) and superscript (h) implies that it has been evaluated for the perturbed metric $h_{\mu\nu}$. The index Eq. (4) implies that these are all four-dimensional geometrical quantities.

Another ingredient in the perturbation of an effective brane-based approach is the perturbation of the bulk Weyl tensor. For that, one has to write down the bulk Weyl tensor in terms of the bulk Riemann, Ricci tensor, and Ricci scalar and expand all of them to leading order in the gravitational perturbation $h_{\alpha\beta}$. The above procedure leads to

$$\begin{aligned} C_{ABCD} &= R_{ABCD} - \frac{1}{3}R_{AC}g_{BD} + \frac{1}{3}R_{AD}g_{BC} + \frac{1}{3}R_{BC}g_{AD} - \frac{1}{3}R_{BD}g_{AC} + \frac{1}{12}R(g_{AC}g_{BD} - g_{AD}g_{BC}) \\ &\simeq C^{(g)}_{ABCD} + \left\{R^{(h)}_{ABCD} - \frac{1}{3}R^{(g)}_{AC}h_{BD} - \frac{1}{3}R^{(h)}_{AC}g_{BD} + \frac{1}{3}R^{(h)}_{AD}g_{BC} + \frac{1}{3}R^{(g)}_{AD}h_{BC} - \frac{1}{3}R^{(h)}_{BD}g_{AC}\right. \\ &\quad - \frac{1}{3}R^{(g)}_{BD}h_{AC} + \frac{1}{3}R^{(h)}_{BC}g_{AD} + \frac{1}{3}R^{(g)}_{BC}h_{AD} + \frac{1}{12}R^{(h)}(g_{AC}g_{BD} - g_{AD}g_{BC}) \\ &\quad \left. + \frac{1}{12}R^{(g)}(g_{AC}h_{BD} + h_{AC}g_{BD} - g_{AD}h_{BC} - h_{AD}g_{BC})\right\}. \end{aligned} \tag{9}$$

Here, superscript (g) indicates that the respective quantity is evaluated for the bulk background metric g_{AB}. Note that due to the dependence of $q_{\alpha\beta}$ on an extra-dimensional coordinate y, quantities evaluated for the bulk metric will inherit y derivatives of $q_{\alpha\beta}$ and hence will differ from their four-dimensional counterparts. Given the perturbation of the bulk Weyl tensor, the corresponding projection of the perturbed bulk Weyl tensor onto the brane hypersurface results in

$$\begin{aligned} E_{\mu\nu} \simeq E^{(g)}_{\mu\nu} + \Big\{ & R^{(h)}_{ABCD}e^A_\mu n^B e^C_\nu n^D - \frac{1}{3}R^{(h)}_{AC}e^A_\mu e^C_\nu \\ & - \frac{1}{3}R^{(h)}_{BD}n^B n^D q_{\mu\nu} - \frac{1}{3}R^{(g)}_{BD}n^B n^D h_{\mu\nu} \\ & + \frac{1}{12}R^{(h)}q_{\mu\nu} + \frac{1}{12}R^{(g)}h_{\mu\nu}\Big\}. \end{aligned} \tag{10}$$

Note that, in the above perturbation equation for the projected bulk Weyl tensor, the first-order corrections to the bulk Riemann, Ricci tensor, and Ricci scalar appears. One can decompose all these perturbed quantities evaluated for the bulk metric in terms of the respective brane metric and extra-dimensional contributions. This has been explicitly carried out in Appendix A and ultimately leads to the following expression for the projected bulk Weyl tensor,

$$\begin{aligned} E^{(h)}_{\mu\nu} = & \frac{1}{6}\,{}^{(4)}\Box h_{\mu\nu} - \frac{1}{3}\partial_y^2 h_{\mu\nu} - k\partial_y h_{\mu\nu} + \frac{1}{3}k^2 h_{\mu\nu} \\ & + \frac{1}{3}h^{\alpha(4)}_\beta R^{(q)\beta}{}_{\mu\alpha\nu} - \frac{1}{6}h^{\alpha(4)}_\mu R^{(q)}_{\alpha\nu} \\ & - \frac{1}{6}h^{\alpha(4)}_\nu R^{(q)}_{\alpha\mu} + \frac{1}{12}\,{}^{(4)}R^{(q)}h_{\mu\nu}. \end{aligned} \tag{11}$$

At this stage, it is worth emphasizing that the gauge conditions elaborated in Eq. (5) take a simpler form in this context. In particular, the spatial part of the differential condition $\nabla_A h^A_\mu = 0$, when expanded in terms of four-dimensional quantities, immediately yields $\nabla_\nu h^\nu_\mu = 0$. Use

of this relation and the commutator of a four-dimensional covariant derivative results in $\nabla^{\mu}E^{(h)}_{\mu\nu}=0$, as is evident from Eq. (11) in the context of vacuum solutions.

One can also try to understand this result from a different perspective. Because we are perturbing around vacuum solutions, it follows from Eq. (2) that $E^{(h)}_{\mu\nu}\propto {}^{(4)}G^{(h)}_{\mu\nu}$. Thus it immediately implies that $\nabla_{\mu}E^{(h)\mu\nu}=0$, as it should be, by virtue of Bianchi identity. Finally, collecting all of the pieces from perturbation of the bulk Weyl tensor elaborated in Eq. (11) as well as the perturbation of the original Einstein tensor as in Eq. (8), we obtain

$$e^{2ky}\{{}^{(4)}\Box h_{\mu\nu}+2h_{\alpha\beta}{}^{(4)}R^{\beta}{}_{\mu}{}^{\alpha}{}_{\nu}\}+\{-k^2h_{\mu\nu}+3k\partial_y h_{\mu\nu}+\partial_y^2 h_{\mu\nu}\}=0. \tag{12}$$

In order to arrive at the above relation, we have used the fact that $q_{\alpha\beta}=\exp(-2ky)g_{\alpha\beta}$, where in this particular situation $g_{\alpha\beta}$ is the Schwarzschild metric. Note that we have not used this fact explicitly anywhere in this section, except for assuming that $g_{\alpha\beta}$ must satisfy vacuum Einstein's equations on the brane. Further, all the geometrical quantities present in the above equation are evaluated for the brane metric $g_{\alpha\beta}$.

At this stage, it is instructive to split the perturbation equations into parts depending on four-dimensional spacetime and those depending on extra dimensions, such that $h_{\alpha\beta}(y,x^{\mu})=h_{\alpha\beta}(x^{\mu})\chi(y)$. Following the separability of the perturbed metric, the above equations can also be decomposed into two parts, which for vacuum brane solution reduce to

$$e^{-2ky}\{-k^2\chi+3k\partial_y\chi+\partial_y^2\chi\}=-\mathcal{M}^2\chi(y), \tag{13}$$

$${}^{(4)}\Box h_{\mu\nu}+2h_{\alpha\beta}{}^{(4)}R^{\alpha}{}_{\mu}{}^{\beta}{}_{\nu}-\mathcal{M}^2h_{\mu\nu}=0. \tag{14}$$

Remarkably, the effect of the whole analysis is just the emergence of a massive gravitational perturbation mode. With $\mathcal{M}=0$, one immediately recovers the dynamical equation governing gravitational perturbation in a nontrivial background. As we will see later, Eq. (13) will lead to a series of masses denoted by m_n and is called the nth Kaluza-Klein mode mass of gravitational perturbation. For each Kaluza-Klein mode, say of order n, there will be a solution $h^{(n)}_{\mu\nu}$ to Eq. (14). When all of these n values are summed, one ends up with the full solution of the gravitational perturbation.

To summarize, we have started from the effective gravitational field equations on the 3-brane, which depends on the bulk Weyl tensor and hence on the bulk geometry. The main problem of this approach is that not all of the components of the projected bulk Weyl tensor $E_{\mu\nu}$ are determined in terms of quantities defined on the brane. In particular, the transverse-traceless part of the projected bulk Weyl tensor, representing the graviton modes in the bulk spacetime, cannot be determined. This is intimately related to the fact that the effective field equations on the brane are *not* closed [75]. In this work, we have circumvented this problem by using the gauge freedom for the gravitational perturbation. We have started with the Schwarzschild anti-de Sitter spacetime [as in Eq. (1)], which identically satisfies the effective gravitational field equations on the brane. We then consider perturbation around this background, which certainly involves graviton modes propagating in the bulk spacetime. However, the use of Randall-Sundrum gauge [presented in Eq. (5)] enables one to reduce the number of propagating degrees of freedom, and hence the effective field equations (at least in the perturbative regime) become closed. Finally, the method of separation of variables enables one to separate a four-dimensional part from the extra-dimensional one and arrives at Eqs. (13) and (14), respectively. The presence of extra dimensions essentially translates into the infinite tower of Kaluza-Klein modes as far as the propagation of gravitational waves in four dimensions is considered.

Let us now emphasise the key differences between our approach and the bulk-based one. Interestingly, Eq. (14) governing the evolution of gravitational perturbation of the four-dimensional brane is identical to that of the bulk-based approach, whereas the eigenvalue equation, i.e., Eq. (13), determining the mass of the graviton is different. Hence the Kaluza-Klein mass modes of graviton in the brane-based approach will be different from that in the bulk-based approach and hence will have interesting observational consequences in both high-energy collision experiments as well as in propagation of gravitational waves. In this work, we will mainly be interested in the effect of the mass term originating from Eq. (14), in particular, how it modifies the behavior of perturbations in contrast to general relativity and also how the brane- and bulk-based approach differs. This is what we will concentrate on in the next sections.

III. SPECIALIZING IN SPHERICALLY SYMMETRIC VACUUM BRANE

We have described a general method for deriving the dynamical equations pertaining to gravitational perturbation, starting from the effective gravitational field equations on the brane in the previous section. We would now like to apply the above scenario in the context of black holes on the brane. In particular, we are interested in perturbations around the background given by Eq. (1). Thus, in this section, with the above scenario in the backdrop, we specialize in vacuum and spherically symmetric solution on the brane, such that $g_{\alpha\beta}=\mathrm{diag}(-f(r),f^{-1}(r),r^2,r^2\sin^2\theta)$. For the moment, we concentrate on situations with arbitrary choices for $f(r)$, whereas later, we will choose a specific form for $f(r)$, namely, $f(r)=1-(2/r)$. Further being a vacuum solution, the Ricci tensor and Ricci scalar identically vanish.

The main focus now will be understanding the evolution equation of the gravitational perturbation $h_{\mu\nu}$ before discussing the Kaluza-Klein modes. In general, the perturbation $h_{\mu\nu}$ can depend on all the spacetime coordinates (t, r, θ, ϕ). The spherical symmetry associated with this problem demands a separation between (t, r) and (θ, ϕ) parts, which results in decomposition of the angular part into spherical harmonics. In particular, for the gravitational perturbation, we obtain

$$h^{(n)}_{\alpha\beta} = \sum_{l=0}^{\infty} \sum_{m=-l}^{l} \sum_{i=1}^{10} h_i^{(nlm)}(t, r)\{Y^{(i)}_{lm}\}_{\alpha\beta}(\theta, \phi), \tag{15}$$

where the perturbation $h_{\alpha\beta}$ has been broken up into ten independent parts, separated into $h_i^{(nlm)}$ depending on (t, r) and the rest depending on the angular coordinates. Further, n stands for the Kaluza-Klein mode index, and l is the angular momentum with m being its z-component. The quantities $\{Y_{lm}\}_{\alpha\beta}$ are the tensorial spherical harmonics in four spacetime dimensions. In order to define these tensor harmonics, one should introduce the following normalized basis vectors:

$$t^\alpha = \frac{1}{\sqrt{f(r)}}(\partial_t)^\alpha; \qquad r^\alpha = \sqrt{f(r)}(\partial_r)^\alpha;$$
$$\theta^\alpha = \frac{1}{r}(\partial_\theta)^\alpha; \qquad \phi^\alpha = \frac{1}{r\sin\theta}(\partial_\phi)^\alpha. \tag{16}$$

It is clear that they are orthogonal to each other, whereas the factors in the front ensure that they are normalized, as well. Given this structure, one can introduce an induced metric on the (θ, ϕ) plane such that $\mu_{\alpha\beta} = g_{\alpha\beta} + t_\alpha t_\beta - r_\alpha r_\beta$, leading to $t^\alpha \mu_{\alpha\beta} = 0 = r^\alpha \mu_{\alpha\beta}$. One can also define an antisymmetric tensor $\epsilon_{\alpha\beta} = \theta_\alpha \phi_\beta - \phi_\alpha \theta_\beta$. Given this, one can construct ten such irreducible representations, which include $t_\alpha t_\beta Y_{lm}$, $\mu_{\alpha\beta} Y_{lm}$ and so on involving no derivatives of Y_{lm}, as well as terms like $r_{(\alpha}\mu_{\beta)\rho}\nabla^\rho Y_{lm}$, $t_{(\alpha}\mu_{\beta)\rho}\nabla^\rho Y_{lm}$ etc. depending on derivatives of Y_{lm}. Among all of these choices, three terms among the ten will depend on the antisymmetric combination $\epsilon_{\alpha\beta}$ and will pick up a term $(-1)^{l+1}$ under parity. These we will refer to as *axial perturbations*. On the other hand, the remaining seven components will inherit an extra factor of $(-1)^l$ under parity transformation and are referred to as *polar perturbations*. Thus the spherical harmonic decomposition of $h^{(n)}_{\alpha\beta}$ in Eq. (15) can be further subdivided into axial and polar parts.

The above decomposition is useful in simplifying the algebra further. It is evident that the operators acting on $h_{\alpha\beta}$ in Eq. (14) are invariant under parity. Thus the solutions to Eq. (14), which are eigenfunctions of parity with different eigenvalues, decouple from each other. Hence, in the present scenario, the polar and axial perturbations differ from each other in parity eigenvalue and hence evolve independently of one another. Further, two axial (or, polar) modes having different l and m values also have different eigenvalues under parity, and hence they also decouple. Thus one can solve for the evolution of a given l mode for axial (or polar) perturbation separately.

Due to the complicated nature of the polar perturbations, we content ourselves with the axial perturbations only. The angular part of the axial perturbations contains essentially three terms: two depend on the single derivative of Y_{lm}, and the third one depends on double derivatives of Y_{lm}. Thus for $l = 0$, all the axial modes identically vanish, and for $l = 1$, the term involving double derivatives of Y_{lm} does not contribute. Hence, in what follows, we will concentrate on the $l \geq 2$ scenario. In this case, there are two master variables which we will denote by $u_{n,l}$ and $v_{n,l}$, and their evolution equations read as follows:

$$\mathcal{D}u_{n,l} + f(r)\left\{m_n^2 + \frac{l(l+1)}{r^2} - \frac{6}{r^3}\right\}u_{n,l} + f(r)\frac{m_n^2}{r^3}v_{n,l} = 0, \tag{17}$$

$$\mathcal{D}v_{n,l} + f(r)\left\{m_n^2 + \frac{l(l+1)}{r^2}\right\}v_{n,l} + 4f(r)u_{n,l} = 0. \tag{18}$$

Here, $\mathcal{D}$ is the differential operator $\partial_t^2 - \partial_{r_*}^2$, where r_* is the tortoise coordinate defined using $f(r)$ as $dr_* = dr/f(r)$. Note that these two differential equations are coupled to each other and provide a complete set. The massless limit also turns out to be interesting. As far as $u_{n,l}$ is concerned, Eq. (17) decouples, and the corresponding potential reduces to the well-known Regge-Wheeler form. The potential for $v_{n,l}$ resembles that of an electromagnetic field. Note that an identical form for the equations was derived in [68], however from a different perspective. This is due to the fact explained in Sec. II; i.e., the evolution of gravitational perturbation equation is identical to [68] modulo of the Kaluza-Klein decomposition and hence the mass term.

Having discussed the scenario for gravitational perturbation, let us explore the higher-dimensional effects, i.e., determination of the mass term by solving Eq. (13). We will be concerned with the even parity eigenfunctions of Eq. (13), as the derivation of effective field equations assumes the existence of Z_2 symmetry. Further, Eq. (13) being a second-order differential equation will require two boundary conditions to uniquely arrive at the solution. Rather than imposing boundary conditions on $\chi(y)$, we will impose boundary conditions in $\partial_y\chi(y)$. Before engaging with the boundary conditions, let us solve Eq. (13), which on introduction of the new variable, $\zeta = e^{ky}$, becomes

$$\zeta^{-2}\left\{-k^2\chi + k^2\zeta^2\frac{d^2\chi}{d\zeta^2} + 4k^2\zeta\frac{d\chi}{d\zeta}\right\} + m^2\chi = 0, \tag{19}$$

where the following results have been used,

$$\frac{d\chi}{dy} = k\zeta\frac{d\chi}{d\zeta}; \qquad \frac{d^2\chi}{dy^2} = k^2\zeta^2\frac{d^2\chi}{d\zeta^2} + k^2\zeta\frac{d\chi}{d\zeta}. \quad (20)$$

One can further transform the above equation to a more manageable form by introducing yet another variable ξ, replacing ζ, such that $m\zeta = \xi$, and the transformed version of Eq. (19) takes the following form,

$$k^2\xi^2\frac{d^2\chi}{d\xi^2} + 4k^2\xi\frac{d\chi}{d\xi} + (\xi^2 - k^2)\chi = 0. \quad (21)$$

The above equation is essentially Bessel's differential equation, and hence its two independent solutions in terms of modified Bessel functions of the first and second kinds are

$$\chi(y) = e^{-\frac{3}{2}ky}\left[C_1 J_\nu\left(\frac{me^{ky}}{k}\right) + C_2 Y_\nu\left(\frac{me^{ky}}{k}\right)\right], \quad (22)$$

with $\nu = \sqrt{13}/2$. The departure from a bulk-based approach should now be evident from the above analysis. The effect of higher dimensions is through the extra-dimensional part of the gravitational perturbation, namely $\chi(y)$. This is certainly a discriminating feature between the bulk- and the brane-based approaches as the order of the Bessel functions appearing in these two approaches to determine the Kaluza-Klein mode masses is different [68]. Thus it is clear that the mass spectrum of our model will be different than that of the bulk-based approach.

Let us briefly point out the reason behind the difference between Kaluza-Klein mode masses when one follows the brane-based approach, on the one hand, and the bulk-based approach, on the other hand. This is basically due to the difference in the gravitational field equations. For example, when perturbing the bulk gravitational field equations, the Weyl tensor plays no role. By contrast, the perturbation of the Weyl tensor plays a central role in the brane-based approach. Therefore, the basic field equations governing dynamics of gravity in the two approaches differ, but the Schwarzschild anti-de Sitter spacetime is still a solution of both of the field equations. Hence, even though the background solution is the same in both cases, the perturbations follow different dynamics pertaining to the fact that field equations themselves are different. This is why the Kaluza-Klein mode masses are also different. An analogy may be helpful here. For instance, the Schwarzschild solution is a solution of both Einstein gravity as well as $f(R)$ gravity. However, the field equations of both these theories are widely different. Thus, the perturbations about the Schwarzschild background will satisfy different evolution equations in these theories (see, for example, [16,85,86]), like the scenario we are considering in this work. The fact that the field equations in the bulk- and brane-based approaches are different is known and is manifested in the fact that there exist solutions to the field equations in the brane-based approach, with no bulk correspondence whatsoever [81,82,84,87,88]. This explains the difference in the masses of the Kaluza-Klein modes associated with the brane- and the bulk-based approaches.

To find the unknown coefficients C_1 and C_2, we need to impose boundary conditions, and as emphasized earlier, these conditions will be on derivatives of $\chi(y)$. To make the analysis on par with possible resolutions of the hierarchy problem, we assume the existence of another brane located at $y = d$. Incidentally, the distance d need not be constant but varying, known as radion field, whose stabilization would lead to a nonzero interbrane separation d [36]. We have also neglected effects of brane bending, if any, by assuming that d is a pure constant. Hence, the boundary conditions imposed are given by $[\partial_y + (\nu + (3/2))k]\chi = 0$ at $y = 0$ and also on the other brane hypersurface at $y = d$. This leads to the following two algebraic equations satisfied by the two unknown coefficients C_1 and C_2 as

$$C_1 J_{\nu-1}(m/k) + C_2 Y_{\nu-1}(m/k) = 0, \quad (23)$$

$$C_1 J_{\nu-1}(\{m/k\}e^{kd}) + C_2 Y_{\nu-1}(\{m/k\}e^{kd}) = 0. \quad (24)$$

Using the first relation, one can determine the ratio C_1/C_2, and hence, the solution for $\chi(y)$ is determined except for an overall normalization. On the other hand, substitution of the same in Eq. (24) results in the algebraic equation

$$Y_{\nu-1}(m_n/k)J_{\nu-1}(z_n) - J_{\nu-1}(m_n/k)Y_{\nu-1}(z_n) = 0, \quad (25)$$

where $m_n = \{z_n k\}e^{-kd}$ yields an infinite series of solutions for the mass, where n stands for a particular Kaluza-Klein mode. The masses for the first ten Kaluza-Klein modes have been presented in Table I for two different sets of choices of interbrane separation d and bulk curvature scale $\ell = 1/k$. This has been achieved by first solving for z_n using Eq. (25) and then obtaining the Kaluza-Klein mass m_n.

To see clearly the difference between brane- and bulk-based approaches, we have presented the masses of the first ten lowest-lying Kaluza-Klein modes in the context of the bulk-based approach, as well. This requires solving Eq. (25) for z_n with $\nu = 2$. It is evident from Table II that the solutions for z_n are completely different in the two scenarios. In particular, the numerical values of z_n in the brane-based approach are lower than the corresponding numerical values in the bulk-based approach. This results in lowering of the masses of Kaluza-Klein modes in the brane-based approach, as evident from Tables I and II for the choices $d/\ell = 20$ and $\ell^{-1} = 6 \times 10^7$ in geometrized units. The numerical values are so chosen that they are in agreement with other constraints already present in this framework. For example, $d/\ell \geq 13$ is necessary to arrive at

TABLE I. Numerical estimates of the first ten Kaluza-Klein mass modes correct to the second decimal place for two possible choices of the interbrane separation d and bulk curvature scale ℓ have been presented for brane-based approach. First, Eq. (25) has been solved for z_n, and the result has been presented in the second column. Incidentally, the solution for z_n is insensitive to choices of d/ℓ as far as solutions accurate to second decimal places are considered. To avoid any instability present in the problems, the inverse of the bulk curvature scale has been chosen such that the mass of the lowest-lying Kaluza-Klein mode is greater than or equal to 0.43 in geometrized units.

Kaluza-Klein modes	z_n	Associated mass $(d/\ell = 20;\ 1/\ell = 6 \times 10^7)$	Associated mass $(d/\ell = 30;\ 1/\ell = 1.3 \times 10^{12})$
$n = 1$	3.56	0.44	0.43
$n = 2$	6.74	0.83	0.82
$n = 3$	9.88	1.22	1.20
$n = 4$	13.03	1.61	1.58
$n = 5$	16.17	2.00	1.98
$n = 6$	19.32	2.39	2.35
$n = 7$	22.48	2.78	2.73
$n = 8$	25.60	3.17	3.11
$n = 9$	28.75	3.56	3.50
$n = 10$	31.89	3.94	3.88

the desired warping required to get around the gauge hierarchy problem, whereas the table-top experiment of Newton's law would demand $1/\ell \geq 10^7(M/M_\odot)$ (or $\ell \leq 0.1$ mm), where $M_\odot$ is the solar mass [89–91]. This explains the choices of d/ℓ as well as that of $1/\ell$. Numerical estimates of the masses of the Kaluza-Klein modes for two such choices of d/ℓ and $1/\ell$ values have been presented in Tables I and II, respectively. Masses of these Kaluza-Klein modes will be used in the next section for determination of the quasinormal modes for the brane black hole.

TABLE II. Numerical estimates of the mass of first ten Kaluza-Klein modes have been presented for the bulk-based approach, by solving Eq. (25) for $\nu = 2$. It is clear from I that the solution z_n of Eq. (25) is different in the bulk-based approach in comparison to the brane-based one. Among the two sets of choices for the interbrane separation d and bulk curvature scale ℓ, one is identical to that of the brane-based approach, whereas the other slightly differs. Both of these situations clearly depict the differences of the Kaluza-Klein mass modes in the brane- and the bulk-based approaches.

Kaluza-Klein modes	z_n	Associated mass $(d/\ell = 20;\ 1/\ell = 6 \times 10^7)$	Associated mass $(d/\ell = 30;\ 1/\ell = 1.2 \times 10^{12})$
$n = 1$	3.83	0.47	0.43
$n = 2$	7.01	0.87	0.79
$n = 3$	10.18	1.26	1.14
$n = 4$	13.33	1.65	1.50
$n = 5$	16.46	2.03	1.85
$n = 6$	19.61	2.42	2.20
$n = 7$	22.76	2.81	2.56
$n = 8$	25.91	3.20	2.91
$n = 9$	29.05	3.59	3.26
$n = 10$	32.19	3.98	3.61

At this stage, it is worth mentioning the Gregory-Laflamme instability, which originates due to instability of the bulk metric under perturbation pertaining to long wavelength modes [20,92–95]. The fact that there exists another brane at $y = d$ helps to evade the instability by providing a cutoff on the long wavelength modes. The separation d between the two branes as well as the bulk curvature scale $\ell \sim 1/k$ [see Eq. (1)] is also bounded by the fact that we have not seen any influence of the extra dimension on the gravitational interaction in our observable universe. The above instability essentially translates through d and ℓ into the mass of the Kaluza-Klein modes, and for $m_n \gtrsim 0.43$, the above instability can be avoided, which is also reflected in both the tables depicting masses of the Kaluza-Klein modes (see also [96]).

Finally, given a particular Kaluza-Klein mode n, one can determine the extra-dimensional part of the gravitational perturbation as

$$\chi_n(y) = N_n[Y_{\nu-1}(m_n/k)J_\nu(\{m_n/k\}e^{ky}) - J_{\nu-1}(m_n/k)Y_\nu(\{m_n/k\}e^{ky})]. \tag{26}$$

Here, N_n is the overall normalization factor, and $\nu = \sqrt{13}/2$ is the order of the Bessel functions. Thus, the complete solution to the gravitational perturbation can be written in the following form,

$$h_{\alpha\beta}(t,r,\theta,\phi;y) = \sum_{n=0}^{\infty} N_n\{Y_{\nu-1}(m_n/k)J_\nu(\{m_n/k\}e^{ky}) - J_{\nu-1}(m_n/k)Y_\nu(\{m_n/k\}e^{ky})\} \times \sum_{l=0}^{\infty}\sum_{m=-l}^{l}\left\{\sum_{i=1}^{7} P_i^{(nlm)}(t,r)\mathcal{P}_{\alpha\beta}^{(i)lm}(\theta,\phi) + \sum_{i=1}^{3} A_i^{(nlm)}(t,r)\mathcal{A}_{\alpha\beta}^{(i)lm}(\theta,\phi)\right\}. \tag{27}$$

Here, the first part is the contribution from extra dimensions, whereas the four-dimensional effects have been divided into polar and axial perturbations. The first seven are the polar perturbations, and the last three are the axial ones. As already emphasized earlier, these two contributions do not mix, and hence, one can treat them separately. We have already provided the evolution equations for the master variables associated with the axial perturbation in Eqs. (17) and (18), which we will solve next. The solution (or evolution) can be obtained in two ways: by calculating quasinormal modes or by performing a fully numerical Cauchy evolution of the initial data. We have performed

both of these analysis in this work and shall present the calculation of quasinormal modes in the next section before taking up the Cauchy evolution of initial data.

IV. SPECTRUM OF ASSOCIATED QUASINORMAL MODES

In this section, we will investigate the characteristic frequencies, namely, the quasinormal modes associated with the propagation of massive Kaluza-Klein modes in the Schwarzschild geometry induced on the brane hypersurface. This is usually performed by going over to the frequency space, such that

$$u_{n,l}(t,r) = \int d\omega e^{-i\omega t}\psi_{n,l}(\omega,r), \tag{28}$$

$$v_{n,l}(t,r) = \int d\omega e^{-i\omega t}\phi_{n,l}(\omega,r). \tag{29}$$

At this stage, all possible frequencies are allowed, but as we will see later, this is not the case. Only some specific sets of frequencies are allowed, known as the quasinormal mode frequencies, and hence the above integral will be converted to a sum over all the quasinormal mode frequencies. The single most important fact about this expansion is that the quasinormal mode frequencies can be imaginary. Because we do not expect any runaway situations associated with this problem, thus $\mathrm{Im}(\omega) < 0$ are the allowed quasinormal mode frequencies [64,97–105]. Before getting into the details of obtaining the quasinormal mode frequencies in this context, let us briefly discuss another prediction of Eqs. (17) and (28), namely late time wave tails. Because quasinormal mode frequencies have real as well as imaginary parts, it is exponentially suppressed, and at late times ($t \to \infty$), it produces vanishing contribution. Therefore, the wave tail, originating from the existence of a branch cut in the frequency integral of Eq. (28), dominates the late time behavior of the gravitational perturbation $u_{n,l}(t)$. It turns out that the power law scaling of the perturbation modes has a universal behavior. In particular, for massive gravitational modes, which includes the scenario presented in this work, the late time behavior essentially corresponds to the following universal power law behavior, $u_{n,l}(t) \sim t^{-5/6}\sin(\omega t)$. Here, the oscillation frequency ω depends on the mass of the perturbation mode linearly. Thus, the late time behavior is essentially governed by the $t^{-5/6}$ universal factor. We will need this fact in the later parts of this work. For the moment, we will exclusively concentrate on the quasinormal mode analysis.

In order to determine the quasinormal mode frequencies, one also needs to impose suitable boundary conditions on the solution space. These are as follows: (a) the quasinormal mode must be ingoing at the black hole horizon, and (b) these modes must be outgoing in the asymptotic regions. These conditions are best suited in terms of the tortoise coordinate r_*, defined as the integral of $\{dr/f(r)\}$, in which the horizon corresponds to $r_* \to -\infty$, and the asymptotic region implies $r_* \to \infty$. Thus, the condition where quasinormal modes are ingoing at the horizon implies that $u_{n,l}(\omega, r_*)$ and $v_{n,l}(\omega, r_*)$ behave as $\exp(-i\omega r_*)$ in the near horizon regime. A similar situation will exist for the asymptotic region, as well. These boundary conditions will dictate the discrete values of the frequencies associated with the quasinormal modes. These values will have three indices: the Kaluza-Klein mode index n, the angular momentum index l, and the quasinormal mode index p. Having obtained the corresponding quasinormal modes, one can substitute them back to Eqs. (28) and (29) and thus obtain the time evolution of both $u_{n,l}(t, r_*)$ and $v_{n,l}(t, r_*)$. These estimates can then be compared with the Cauchy evolution problem, and a match between the two will ensure correctness of our method presented here. Thus, for completeness and consistency, we will also present results for the Cauchy evolution in the next section. We will mainly content ourselves with the continued fraction method but will briefly discuss the forward integration scheme, as well.

A. Continued fraction method

The frequency spectrum associated with the quasinormal modes can be obtained by starting with a suitable ansatz for $u_{n,l}(t,r)$ and $v_{n,l}(t,r)$. Given this ansatz, one can try to obtain a power series solution associated with the differential equations presented in Eqs. (17) and (18), resulting in a recursion relation between the coefficients of various terms in the power series. This recursion relation will be satisfied provided the quasinormal mode frequencies are discrete. For this purpose, we start with the following general form of the coupled differential equations:

$$-\frac{\partial^2 u_{n,l}}{\partial t^2} + \frac{\partial^2 u_{n,l}}{\partial r_*^2} - f(r)\left(m_n^2 + \frac{l(l+1)r-6}{r^3}\right)u_{n,l} - f(r)\frac{m_n^2}{r^3}v_{n,l} = 0, \tag{30}$$

$$-\frac{\partial^2 v_{n,l}}{\partial t^2} + \frac{\partial^2 v_{n,l}}{\partial r_*^2} - f(r)\left(m_n^2 + \frac{l(l+1)}{r^2}\right)v_{n,l} - 4f(r)u_{n,l} = 0, \tag{31}$$

where $f(r) = 1 - (2/r)$. Subsequently eliminating derivatives with respect to r_* in favor of r and writing down the two master variables $u_{n,l}(t,r)$ and $v_{n,l}(t,r)$ as in Eqs. (28) and (29), we obtain after simplifications

$$r(r-2)\frac{d^2\psi_{n,l}}{dr^2} + 2\frac{d\psi_{n,l}}{dr} + \frac{\omega^2 r^3}{r-2}\psi_{n,l} - \left[m_n^2 r^2 + l(l+1) - \frac{6}{r}\right]\psi_{n,l} - \frac{m_n^2}{r}\phi_{n,l} = 0, \tag{32}$$

$$r(r-2)\frac{d^2\phi_{n,l}}{dr^2}+2\frac{d\phi_{n,l}}{dr}+\frac{\omega^2 r^3}{r-2}\phi_{n,l} - [m_n^2 r^2+l(l+1)]\phi_{n,l}-4r^2\psi_{n,l}=0. \quad (33)$$

Having derived the basic equations governing $\psi_{n,l}$ and $\phi_{n,l}$, one normally writes down both of these master variables in terms of various powers of r and $(r-2)$, such that the boundary conditions at the horizon and at asymptotic regions can be satisfied. Subsequently, the remaining pieces of $\psi_{n,l}$ and $\phi_{n,l}$ are solved by using the power series method. The resulting recursion relation between the coefficients of these power series will also be coupled, and it is only helpful to combine them into a single matrix equation with off-diagonal entries illustrating the coupling between the systems. Performing the same for the master variables involved here, as well, one ends up with the following matrix equation for $j>0$, with integer j as

$$\mathbf{P}_j\mathbf{V}_{j+1}+\mathbf{Q}_j\mathbf{V}_j+\mathbf{R}_j\mathbf{V}_{j-1}=0. \quad (34)$$

Here, the coefficients $\mathbf{P}_j$, $\mathbf{Q}_j$, and $\mathbf{R}_j$ depend on the details of the system, i.e., on the parameters involved. The vector $\mathbf{V}_j$, on the other hand, corresponds to a column matrix constructed out of the power series coefficients for $\psi_{n,l}$ and $\phi_{n,l}$, such that one obtains

$$\mathbf{P}_j=\begin{pmatrix}\alpha_j & 0\\ 0 & \alpha_j\end{pmatrix},\qquad \mathbf{Q}_j=\begin{pmatrix}\beta_j+3 & -\frac{m_n^2}{2}\\ -4 & \beta_j\end{pmatrix},$$
$$\mathbf{R}_j=\begin{pmatrix}\gamma_j-3 & \frac{m_n^2}{2}\\ 0 & \gamma_j\end{pmatrix}, \quad (35)$$

where the unknown coefficients α_j, β_j, and γ_j can be written in terms of the Kaluza-Klein mode mass and the quasinormal mode frequency ω as

$$\alpha_j=(j+1)(j+1-4i\omega),$$
$$\gamma_j=\left(j-1+\frac{(\omega-i\lambda)^2}{\lambda}\right)\left(j+1+\frac{(\omega-i\lambda)^2}{\lambda}\right),$$
$$\beta_j=-2j^2+\left(-2+\frac{8i\omega\lambda-2\omega^2+6\lambda^2}{\lambda}\right)j - l(l+1)+\frac{1}{\lambda}(3\lambda^2-\omega^2-12i\omega\lambda^2-4\lambda^3 + 4i\omega\lambda+12\lambda\omega^2+4i\omega^3). \quad (36)$$

where $\lambda=\sqrt{m_n^2-\omega^2}$. The above recursion relation must be supplemented with the zeroth-order recursion relation, which simply reads $\mathbf{P}_0\mathbf{V}_1+\mathbf{Q}_0\mathbf{V}_0=0$. Given this, one can use Eq. (34) to replace $\mathbf{V}_1$ in terms of $\mathbf{V}_0$ and $\mathbf{V}_2$. Subsequently, one can again replace $\mathbf{V}_2$ by higher-order terms using Eq. (34) repeatedly. This method of solving the matrix valued recursion relation presented in Eq. (34) is known as the method of continued fraction. In this method, following the procedure outlined above, one ends up with an equation of the form $\mathbf{M}\mathbf{V}_0=0$, where the matrix $\mathbf{M}$ reads

$$\mathbf{M}=\mathbf{Q}_0-\mathbf{P}_0[\mathbf{Q}_1-\mathbf{P}_1\{\mathbf{Q}_2+\mathbf{P}_2\mathbf{M}_2\}\mathbf{R}_2]^{-1}\mathbf{R}_1. \quad (37)$$

Here, $\mathbf{M}_j$ is a matrix which can be written in terms of $\mathbf{P}_{j+1}$, $\mathbf{Q}_{j+1}$, $\mathbf{R}_{j+1}$ and most importantly also depends on $\mathbf{M}_{j+1}$. Moreover, the matrix $\mathbf{M}_j$ when acting on $\mathbf{V}_j$ yields $\mathbf{V}_{j+1}$. Thus, in order for the matrix equation $\mathbf{M}\mathbf{V}_0=0$ to have nontrivial solutions for $\mathbf{V}_0$, one must have

$$\det\mathbf{M}=0. \quad (38)$$

In principle, one needs to take into account an infinite number of terms to solve the above equation. However, in practice, one truncates $\mathbf{M}_j$ at some order J and, hence, obtains all the lower-order matrices starting from $\mathbf{M}_J$. Of course, at a later stage, one needs to check the independence of the solution of Eq. (38) explicitly on the truncation order J. We have solved the above matrix valued recursion relation using the continued fraction method discussed earlier in the symbolic manipulation package MATHEMATICA and have obtained the corresponding lowest-lying quasinormal mode frequencies associated with various Kaluza-Klein mode masses for different values of angular momentum. These values are listed in four tables. In Table III, we present both the real and imaginary parts of the quasinormal mode frequencies for the two lowest-lying Kaluza-Klein mass modes associated with the following values: $d/\ell=20$; $1/\ell=6\times10^7$. It is clear that as the mass increases the imaginary part of the lowest quasinormal mode frequency decreases, whereas it increases with angular momentum. For example, when $l=2$, $\mathrm{Im}\omega=-0.05$ for $m_1=0.44$, and it becomes -0.04 as the mass increases to $m_2=0.83$. Hence, the more massive the Kaluza-Klein modes are, the quasinormal mode functions are less and less damped, a feature in complete agreement with the result of [68]. Although for $m=0.44$, the imaginary part of the lowest quasinormal mode frequency will read $\mathrm{Im}\omega=-0.051$ for $l=2$, and it becomes -0.078 as the angular momentum increases to $l=3$. Thus, with an increase of angular momentum, the imaginary part of the quasinormal mode frequency also increases. Hence, among the modes with $l=2$ and $l=3$, the time evolution of the $l=3$ mode will be more damped in comparison to that of the $l=2$ one. This feature is also present in Table IV, where the quasinormal mode frequencies have been presented for a different choice of the ratio between brane separation and bulk curvature scale, namely, for $d/\ell=30$ and $1/\ell=1.3\times10^{12}$.

These numerical values are again chosen to be consistent with previous experimental bounds on d and ℓ as explained earlier. In this case also, as the mass of the Kaluza-Klein

TABLE III. Real and imaginary parts of the quasinormal mode frequencies have been presented. These are obtained from the *brane-based approach* with the following choice of parameters associated with the extra dimensions: $d/\ell = 20$; $1/\ell = 6 \times 10^7$. In particular, results for the first two Kaluza-Klein mass modes have been presented for four different choices of the angular momentum.

	$m = 0.44,\ l = 2$		$m = 0.83,\ l = 2$	
Mode	Real	Imaginary	Real	Imaginary
$j = 1$	0.467	−0.051	0.396	−0.038
$j = 2$	0.530	−0.071	0.543	−0.104
$j = 3$	0.378	−0.197	0.183	−0.168
$j = 4$	0.473	−0.239	0.243	−0.369
	$m = 0.44,\ l = 3$		$m = 0.83,\ l = 3$	
$j = 1$	0.653	−0.078	0.843	−0.051
$j = 2$	0.708	−0.084	0.708	−0.134
$j = 3$	0.618	−0.244	0.773	−0.176
$j = 4$	0.562	−0.437	0.576	−0.327
	$m = 0.44,\ l = 4$		$m = 0.83,\ l = 4$	
$j = 1$	0.847	−0.086	0.951	−0.064
$j = 2$	0.827	−0.263	0.960	−0.219
$j = 3$	0.791	−0.451	0.896	−0.393
	$m = 0.44,\ l = 5$		$m = 0.83,\ l = 5$	
$j = 1$	1.043	−0.090	1.123	−0.076
$j = 2$	1.084	−0.272	−1.098	−0.233
$j = 3$	1.002	−0.460	1.051	−0.404

TABLE IV. Real and imaginary parts of the first few quasinormal mode frequencies have been depicted. These values are obtained starting from the *brane-based approach*, with the following choices of the extra-dimensional parameters: $d/\ell = 30$; $1/\ell = 1.3 \times 10^{12}$. Results have been presented for the two lowest-lying Kaluza-Klein mass modes and for four choices of angular momentum associated with each modes.

	$m = 0.43,\ l = 2$		$m = 0.82,\ l = 2$	
Mode	Real	Imaginary	Real	Imaginary
$j = 1$	0.462	−0.053	0.702	−0.006
$j = 2$	0.527	−0.072	0.385	−0.041
$j = 3$	0.377	−0.201	0.541	−0.109
$j = 4$	0.471	−0.241	0.253	−0.326
	$m = 0.43,\ l = 3$		$m = 0.82,\ l = 3$	
$j = 1$	0.650	−0.079	0.796	−0.036
$j = 2$	0.616	−0.246	0.705	−0.138
$j = 3$	0.679	−0.261	0.770	−0.179
$j = 4$	0.562	−0.439	0.576	−0.331
	$m = 0.43,\ l = 4$		$m = 0.82,\ l = 4$	
$j = 1$	0.846	−0.086	0.948	−0.065
$j = 2$	0.826	−0.264	0.906	−0.204
$j = 3$	0.790	−0.452	0.833	−0.373
	$m = 0.43,\ l = 5$		$m = 0.82,\ l = 5$	
$j = 1$	1.041	−0.090	1.120	−0.076
$j = 2$	1.027	−0.272	1.095	−0.234
$j = 3$	1.001	−0.461	1.050	−0.406

TABLE V. Numerical estimates for real and imaginary parts of the quasinormal mode frequencies obtained from the *bulk-based approach*. The parameters characterizing the bulk spacetime corresponds to $d/\ell = 20$; $1/\ell = 6 \times 10^7$. In this situation, as well we have presented the quasinormal mode frequencies for four possible choices of angular momentum given the two lowermost Kaluza-Klein mode masses.

	$m = 0.47,\ l = 2$		$m = 0.87,\ l = 2$	
Mode	Real	Imaginary	Real	Imaginary
$j = 1$	0.480	−0.046	0.437	−0.015
$j = 2$	0.540	−0.067	0.542	−0.087
$j = 3$	0.381	−0.185	0.119	−0.128
$j = 4$	0.477	−0.231	0.242	−0.318
	$m = 0.47,\ l = 3$		$m = 0.87,\ l = 3$	
$j = 1$	0.660	−0.076	0.862	−0.045
$j = 2$	0.716	−0.082	0.719	−0.117
$j = 3$	0.623	−0.239	0.785	−0.163
$j = 4$	0.564	−0.431	0.576	−0.313
	$m = 0.47,\ l = 4$		$m = 0.87,\ l = 4$	
$j = 1$	0.853	−0.085	1.010	−0.067
$j = 2$	0.831	−0.259	0.920	−0.193
$j = 3$	0.793	−0.447	0.840	−0.359
	$m = 0.47,\ l = 5$		$m = 0.87,\ l = 5$	
$j = 1$	1.047	−0.089	1.176	−0.077
$j = 2$	1.032	−0.269	1.108	−0.227
$j = 3$	1.004	−0.457	1.058	−0.396

mode increases, the imaginary part of the quasinormal mode frequency decreases, and the increase of angular momentum has a reverse effect. For the same choices of the bulk parameters, the Kaluza-Klein mode masses for the brane-based and the bulk-based approaches differ, as evident from Tables I and II. For example, in the situation where $d/\ell = 20$; $1/\ell = 6 \times 10^7$, the lowest-lying Kaluza-Klein mode mass in the brane-based approach is $m_1 = 0.44$, whereas that in the bulk-based approach is $m_1 = 0.47$. Hence, the imaginary part of the quasinormal mode frequency will be lower for the bulk-based approach. This has interesting implications: the axial perturbation generated from bulk Einstein's equations will decay at a slower pace in time when compared to the corresponding perturbation mode that originates from effective field equations on the brane. This situation has been clearly depicted in Tables V and VI, respectively (see also Fig. 1). One can also check that the quasinormal mode frequencies derived here indeed match those derived in the direct integration scheme, which we will discuss next.

B. Direct integration method

In the previous section, we discussed one particular method of determining the quasinormal mode frequencies associated with the perturbation of brane world black hole. However, for completeness, we present another

TABLE VI. Real and imaginary parts of the quasinormal mode frequencies have been depicted in a bulk spacetime with the following set of parameters: $d/\ell = 30$; $1/\ell = 1.2 \times 10^{12}$ in the *bulk-based approach*. The values have been presented for four choices of angular momentum, given the two lowest-lying Kaluza-Klein modes.

	$m = 0.43,\ l = 2$		$m = 0.79,\ l = 2$	
Mode	Real	Imaginary	Real	Imaginary
$j = 1$	0.462	−0.053	0.672	−0.006
$j = 2$	0.527	−0.072	0.456	−0.014
$j = 3$	0.377	−0.201	0.542	−0.087
$j = 4$	0.471	−0.241	0.534	−0.123
	$m = 0.43,\ l = 3$		$m = 0.79,\ l = 3$	
$j = 1$	0.650	−0.079	0.825	−0.055
$j = 2$	0.616	−0.246	0.696	−0.149
$j = 3$	0.678	−0.261	0.761	−0.187
$j = 4$	0.562	−0.439	0.666	−0.377
	$m = 0.43,\ l = 4$		$m = 0.79,\ l = 4$	
$j = 1$	0.846	−0.086	0.937	−0.067
$j = 2$	0.826	−0.264	0.898	−0.210
$j = 3$	0.790	−0.452	0.829	−0.382
	$m = 0.43,\ l = 5$		$m = 0.79,\ l = 5$	
$j = 1$	1.041	−0.090	1.112	−0.078
$j = 2$	1.027	−0.272	−1.089	−0.238
$j = 3$	1.001	−0.461	1.045	−0.411

supplementary method of computing the quasinormal mode frequencies, which can be used along with the continued fraction method to correctly predict the quasinormal mode frequencies. In this method, as the name suggests, one integrates directly from the horizon to the asymptotic region given the boundary conditions mentioned earlier. In this problem, we have two master variables characterizing the axial gravitational perturbation and satisfying two second-order coupled ordinary differential equations [see Eqs. (B5) and (B6), respectively in Appendix B]. The solution in the near horizon regime will have $e^{-i\omega r_*}$ times a power series around the horizon, whereas at infinity, it will behave as $e^{-k_\infty r_*}$, where k_∞ is the wave number in the asymptotic region. The asymptotic solution will be characterized by a two-dimensional column vector $\{b_\infty^{(1)}, b_\infty^{(2)}\}$, for which one can choose a suitable orthonormal system of basis vectors. Numerical integration of these differential equations from the horizon out to infinity will lead to a (2×2) matrix $\mathbf{S}(m_n, \omega)$, which can be expanded in the basis introduced above. Finally, setting the determinant of this matrix $\mathbf{S}$ to zero, one can solve for the quasinormal mode frequencies [101,103].

Further note that this method is particularly suited for determination of quasibound states, for which the leading order behavior of the fields at infinity is well understood. However, for the determination of quasinormal mode frequencies, one needs to extract additional subdominant behavior of the mode functions at infinity, which makes this approach prone to numerical errors. However, if the imaginary part is small compared to the real part, one can determine the quasinormal mode frequencies to sufficient accuracy. In practice, one integrates these differential equations to some high value of radial distance, and the result must be impermeable to any shift in this distance. Also, one can supplement one of these methods by checking whether, for a given Kaluza-Klein mode mass and angular momentum, one obtains the same quasinormal mode frequency from the other. We have explicitly checked that this is indeed the case, and the values obtained from the continued fraction method is in good agreement with those obtained from the direct integration scheme, as well. This depicts the internal consistency of our model in a straightforward manner.

V. NUMERICAL ANALYSIS OF THE QUASINORMAL MODES

The principal aim of this work was to determine the time evolution of the perturbations obtained from the effective gravitational field equations on the brane. Also, we contrast the same with the time evolution of perturbation derived from bulk Einstein's equations. One can achieve this by following two possible avenues: (a) obtaining the quasinormal mode frequencies and hence obtaining the time evolution and (b) solving the Cauchy evolution problem numerically and hence arriving at the evolution of the gravitational perturbation.

In this section, we will follow the first method where the time evolution of the mode function $u_{n,l}(t)$ depicting axial gravitational perturbation will be presented, using the quasinormal mode analysis performed in Section IV. For this purpose, we will use Eq. (28), where the integral over all frequencies will now be replaced by summation over all the quasinormal mode frequencies. Thus, our strategy will be as follows: we will use the numerically computed quasinormal mode frequencies and then sum them in order arrive at the time evolution for the mode function $u_{n,l}(t)$. Here, we would like to reiterate the fact that n stands for the Kaluza-Klein modes, and l is the angular momentum associated with the gravitational perturbation. For example, $u_{0,2}$ corresponds to the axial gravitational perturbation associated with angular momentum $l = 2$ around a general relativity solution, whereas $u_{1,3}$ is the axial gravitational perturbation associated with the lowest-lying Kaluza-Klein mode and with angular momentum $l = 3$. In what follows using the numerical values of quasinormal mode frequencies, we will present the time evolution of $u_{n,l}(t)$ for a few low-lying Kaluza-Klein modes with different choices of angular momentum l. These will be contrasted with the mode functions $u_{0,l}$ associated with general relativity.

Note that this process is inherently approximate because, in principle, one should add all of the quasinormal mode frequencies in order to obtain the time evolution of the

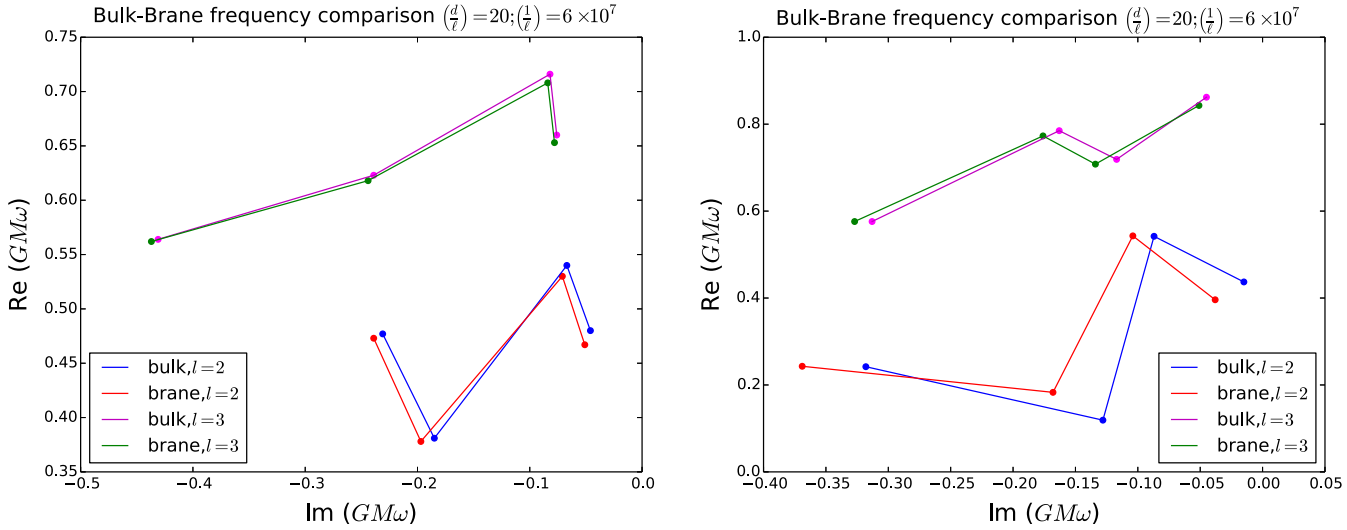

FIG. 1. Real and imaginary parts of the quasinormal mode frequencies have been plotted. The figure on the left corresponds to the quasinormal mode frequencies associated with the lowest-lying Kaluza-Klein mass modes in both the brane- and bulk-based approaches. The curves at the bottom show the $l = 2$ case, and the curves at the top depict the situation when $l = 3$. The figure to the right illustrates an identical situation but for the next Kaluza-Klein mass modes. As evident from the curves, the imaginary part of quasinormal mode frequencies is smaller in the case of the bulk-based approach, resulting in less damping. We will confirm this behavior in the following sections.

perturbation, whereas here, we will consider a few lowest-lying quasinormal modes to perform the same. Even though this is certainly an approximate description, it will nevertheless provide the overall behavior of the gravitational perturbation with time and the key features that will distinguish the scenario presented here from that in general relativity. More refined results can be obtained using the Cauchy evolution, which we will present in the next section. This will provide another self-consistency check of our formalism and hence of the associated results.

As a first step towards the same, we will present the time evolution of the axial perturbation in the context of general relativity alone. This will set the stage for what is to come next. This has been presented in Fig. 2, where we have depicted how the mode functions evolve with time in the actual scale as well as in the logarithmic scale. The

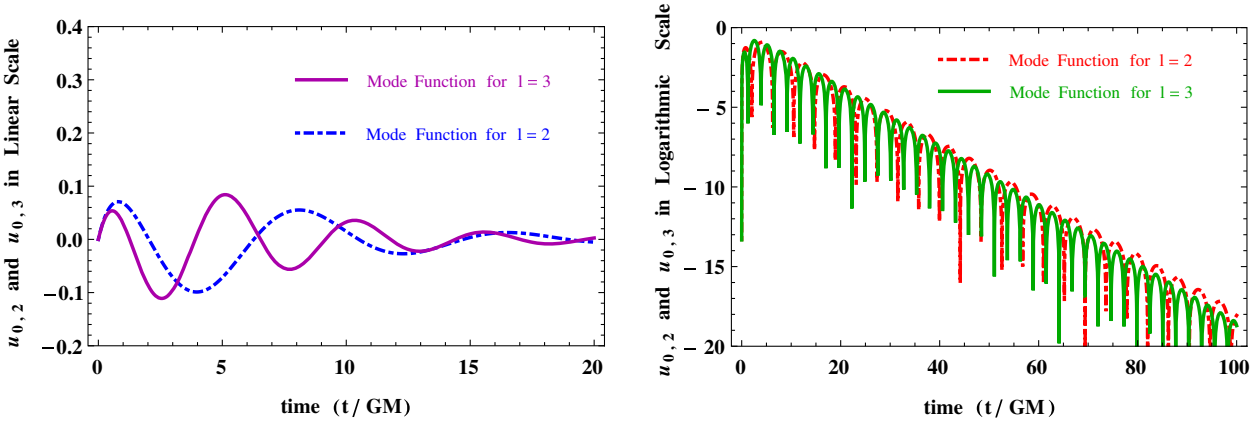

FIG. 2. Time evolution of the master mode function $u_{n,l}(t)$ associated with axial gravitational perturbation for two different values of angular momentum l in the context of general relativity is depicted. The time scale has been normalized to the mass of the central hole, i.e., $t \to t/GM$. Moreover, the figure on the left illustrates the actual evolution of the mode function with time, whereas the right one presents the same but in a logarithmic scale. The amplitude of the mode function corresponding to $l = 3$ is slightly smaller compared to the mode function having $l = 2$, as evident from the right figure. In both of them, the dotted one stands for mode function with $l = 2$, and the continuous one is the mode function with $l = 3$. We will contrast this scenario with the respective ones in the presence of extra dimensions.

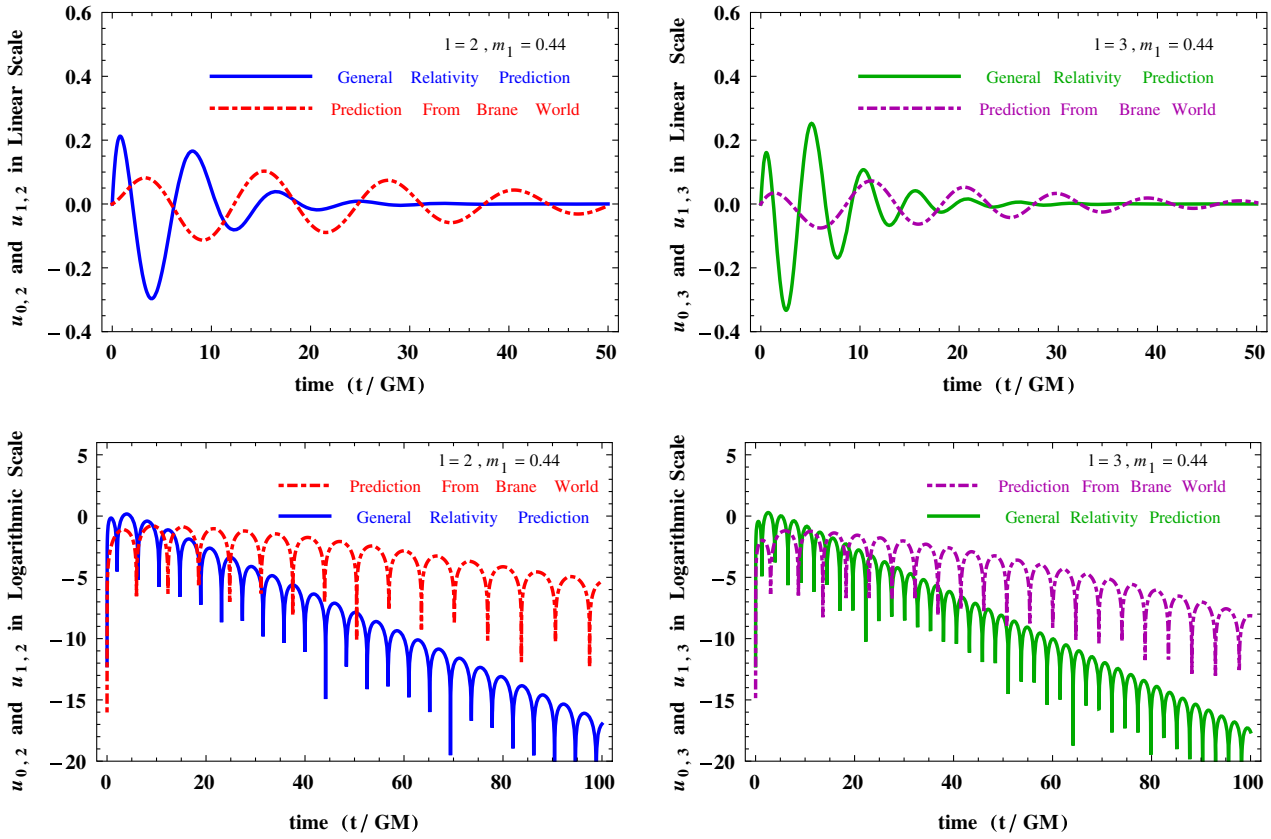

FIG. 3. Time evolution of the master mode function $u_{n,l}(t)$ for two different values of angular momentum both in the context of general relativity ($n = 0$) as well as in the *brane-based approach* is presented. All of the figures are associated with the lowest-lying Kaluza-Klein mode mass $m_1 = 0.44$ (see Table I) but for two different choices of the angular momentum. For brevity, we have presented both: (a) the figures have been drawn in a logarithmic scale (in the bottom panel) and (b) the figures in the actual scale (in the top panel). All of these figures clearly bring out the key differences between these two scenarios. See text for more discussions.

advantage of the logarithmic scale is that it can enhance very tiny differences, with the disadvantage being it will make large differences appear as a small one. The left figure in Fig. 2 presents the actual time evolution of the $l = 2$ and $l = 3$ mode functions in general relativity, i.e., $u_{0,2}(t)$ and $u_{0,3}$, respectively, and the right one presents the same in logarithmic scale. It is clear that there is an appreciable difference between the two at earlier times, which gets washed out as the modes gradually decay. On the other hand, the logarithmic plot shows exactly the opposite nature, as explained earlier.

Returning back to our main goal, we have illustrated time variation of the perturbation associated with the lowest-lying Kaluza-Klein mode having mass $m_1 = 0.44$ and have contrasted the same with general relativity in Fig. 3. The figures on the left depict time variation of the perturbation for $l = 2$ in both actual and logarithmic scale, and those on the right are for $l = 3$. The main difference emerging from Fig. 3 is that the damping time scale of the massive modes is much greater compared to those in general relativity. The same is true for the logarithmic plots, as well, where the fact that modes in general relativity are heavily damped in comparison to the massive modes is very pronounced. The features of the massive modes remain identical to those considered in the second lowest Kaluza-Klein mode having mass $m_2 = 0.83$, as well. Here, the slower decay of the massive modes with time is the key distinguishing feature between general relativity and the higher-dimensional model discussed here.

So far, we have been discussing the time evolution of the gravitational perturbation starting from the effective gravitational field equations on the brane. At this stage, let us try to understand the corresponding situation when the gravitational perturbation originating from the bulk Einstein's equations is being considered. As emphasized earlier, this will be similar to the brane-based approach but will have an associated Kaluza-Klein mass mode, which will be different. For example, as evident from Tables I and II for the same choice of bulk parameters, i.e., $d/\ell = 20$; $1/\ell = 6 \times 10^7$, the Kaluza-Klein mass spectrum will be different in the two scenarios. Thus, in Fig. 4, we have presented the time evolution of the gravitational perturbation derived from the bulk-based approach. Here, we observe the same key features, e.g., very slow decay of

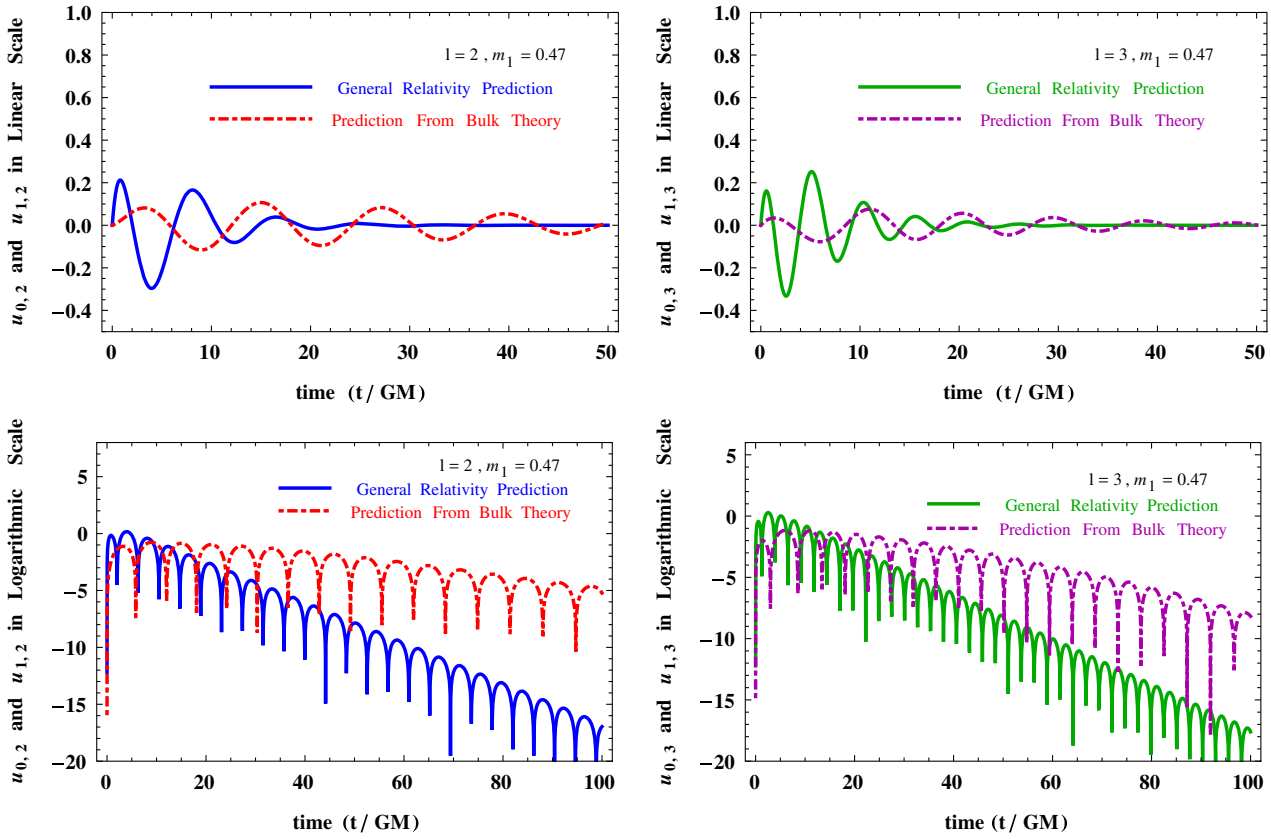

FIG. 4. Top figures depict the time evolution of the master mode function $u_{n,l}(t)$ in the *bulk-based approach* and have been contrasted with that in general relativity ($n = 0$). In this case, behavior of the mode functions in a logarithmic scale and in the actual scale is presented. The Kaluza-Klein mode mass associated with the master variable presented here corresponds to the lowest one with $m_1 = 0.47$ with the following parameters: $d/\ell = 20$; $1/\ell = 6 \times 10^7$.

the perturbation in contrast to that in general relativity. Thus, if the ringdown phase of any black hole merger is being probed for intermediate times, where the evolution of gravitational perturbation is still dominated by the quasinormal modes, any departure from the general relativity prediction can possibly signal the existence of extra spacetime dimensions. Following the general trend, in Fig. 4 as well, we have presented the time evolution in actual as well as in logarithmic scale for two possible choices of angular momentum of $l = 2$ and $l = 3$, respectively.

This enables one to compare the bulk- and the brane-based approach given the same bulk parameters. The resulting discord should be attributed to the difference between the masses of the respective Kaluza-Klein modes. As evident from Fig. 5, this difference is really very small, unlike the situation with general relativity. Moreover, as the masses of the Kaluza-Klein modes are higher in the bulk-based approach, they would decay slower. This can be clearly seen from both the logarithmic plots in Fig. 5, where the perturbation in the bulk-based approach becomes larger than that in the brane-based one at late times. The same features appear for both the angular momentums, as well; however, the difference is much smaller in higher angular momentum compared to the lower one.

All of these features can also be seen for the second lowest Kaluza-Klein mode mass, $m_2 = 0.87$, in the bulk-based approach. The time evolution of the corresponding gravitational perturbation in both actual and logarithmic scale for two choices of the angular momentum shows very similar features when compared with the lowest-lying Kaluza-Klein mass mode. As expected, the massive modes decay very slowly in comparison with general relativity. Further, from the comparison of brane- and bulk-based approaches for the second lowest-lying Kaluza-Klein mode, one may infer that the difference only becomes sensible after a long time has elapsed, and hence if the ringdown phase can be probed minutely at very late times, one may infer the preference of the bulk-based approach over the brane-based one or vice versa. However, the situation is not so simple, and another subtle effect comes into play at late times, which corresponds to the wave tail. All of the quasinormal modes are inherently exponentially suppressed, and hence at very late times, their effects are negligibly small. In this situation, the wave tails enter the picture, and in most cases, the late time behavior is

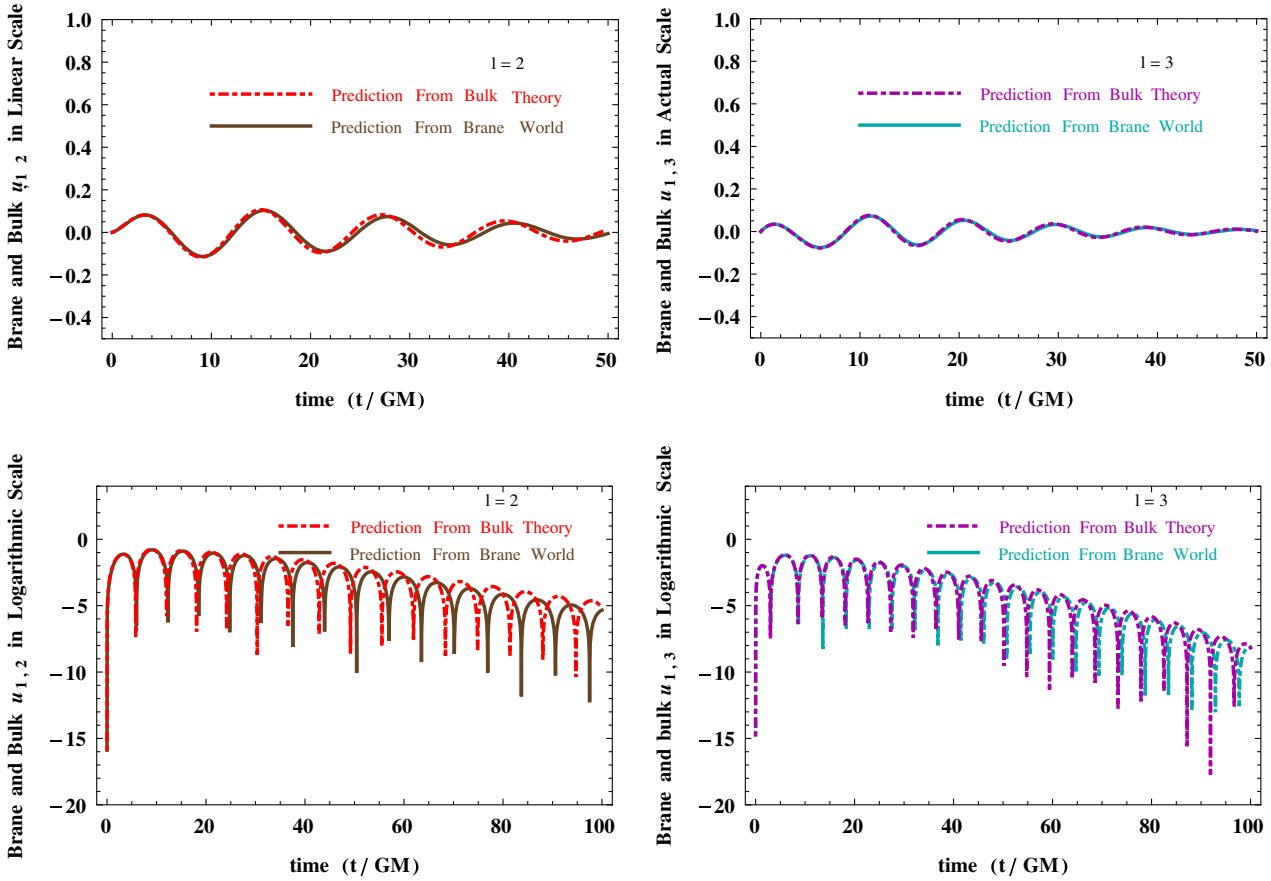

FIG. 5. Two scenarios presented in this work, namely, the perturbation of effective four-dimensional Einstein's equations or the perturbation of bulk Einstein's equations, have been illustrated in this figure, both for the identical choice of the extra-dimensional parameters, i.e., $d/\ell = 20$; $1/\ell = 6 \times 10^7$. It is clear that the time evolution of the mode function $u_{n,l}(t)$ differs from each other in these two distinct approaches. This is primarily due to the difference between the Kaluza-Klein mode masses in these two approaches. See text for more discussions.

essentially governed by the wave tail decaying only as a power law (this is identical to the "bulk-based approach", as well; see [70]). Because the scaling of the power law is mostly universal, independent of the nature of fields and mass of the fields under consideration, both the bulk- and brane-based approaches will decay by an identical power law behavior. This will make the detection of these two different approaches by late time measurements extremely difficult.

VI. CONSISTENCY OF THE APPROACH: COMPARISON WITH CAUCHY EVOLUTION

The previous section illustrates the methods to determine the quasinormal mode frequencies, using the obtained time evolution of the perturbation mode $u_{n,l}$. This is so because, in the limit of $m_n \to 0$ (i.e., general relativity limit), this mode represents the axial gravitational perturbation, whereas the other essentially becomes a gauge degree of freedom. Hence, we can compare the time evolution of $u_{n,l}$ with the respective one in general relativity and see the harmony as well as possible discord among the two. We have already performed the same in the previous section. However, in principle, one expects the above approach to match with the Cauchy evolution of the perturbation equations presented in Eqs. (B5) and (B6), respectively, in Appendix B. This is what we will explore in this section.

For this purpose, we closely follow the analysis put forward in [65] but modifying it wherever necessary. Referring back to Eqs. (17) and (18) as the key differential equations for the master variables, one can write them in a compact manner as

$$\mathcal{D}\mathbf{\Psi} + \mathbf{V}(r)\mathbf{\Psi} = 0. \tag{39}$$

Here, $\mathbf{\Psi}$ is a two-dimensional column matrix constructed from $u_{n,l}$ and $v_{n,l}$. Rather than working with the normal (t, r) coordinates, it is instructive to transform to the light-cone coordinates. The transformation into the light-cone coordinates can be achieved by introduction of the null coordinates as $u = t - r_*$, $v = t + r_*$. Use of these null coordinates modifies Eq. (39) to

$$4\partial_u\partial_v\mathbf{\Psi} + \mathbf{V}(u,v)\mathbf{\Psi} = 0, \tag{40}$$

where

$$\mathbf{\Psi} = \begin{pmatrix} u_{n,l} \\ v_{n,l} \end{pmatrix}, \qquad \mathbf{V} = \begin{pmatrix} V_{11} & V_{12} \\ V_{21} & V_{22} \end{pmatrix}. \tag{41}$$

Here, all the matrix coefficients of $\mathbf{V}$ are dependent on the black hole solution on the brane and the Kaluza-Klein mode mass m_n.

For clarity, we have suppressed the functional dependence of the potential matrix $\mathbf{V}$ for the time being. To proceed further, we need to introduce a notion of a time evolution operator. For this purpose, we note that for an arbitrary function of time $f(t)$, the function given by $e^{h\partial_t}$ is the time evolution operator, in the sense that $e^{h\partial_t}f(t) = f(t+h)$. Thus, in order to obtain the time evolution of the mode functions $\mathbf{\Psi}$, we apply the time evolution operator on Ψ. This yields

$$\mathbf{\Psi}(t+h) = e^{h\partial_t}\mathbf{\Psi} = e^{h\partial_u + h\partial_v}\mathbf{\Psi}. \tag{42}$$

Equation (42) can be written in a nice manner by expanding the right hand side, resulting in

$$\begin{aligned}
\mathbf{\Psi}(u+h,v+h) &= \sum_{j=0}\frac{1}{j!}(h\partial_u)^j \sum_{k=0}\frac{1}{k!}(h\partial_v)^k \Psi(u,v) \\
&= \left[e^{h\partial_u} + e^{h\partial_v} - 1 + \frac{1}{2}h^2\partial_u\partial_v\left(1 + \frac{h\partial_u}{2!} + \frac{h\partial_u{}^2}{3!} + \cdots\right)\left(1 + \frac{h\partial_v}{2!} + \frac{h\partial_v{}^2}{3!} + \cdots\right)\right]\mathbf{\Psi}(u,v) \\
&= \left[e^{h\partial_u} + e^{h\partial_v} - 1 + \frac{1}{2}h^2\partial_u\partial_v\left\{\left(e^{h\partial_u} - (h\partial_u)^2\left(\frac{1}{2!} - \frac{2}{3!}\right) - \cdots\right) + \partial_u \to \partial_v\right\}\right]\mathbf{\Psi}(u,v) \\
&= \left[e^{h\partial_u} + e^{h\partial_v} - 1 + \frac{1}{2}h^2\partial_u\partial_v\{(e^{h\partial_u} + \mathcal{O}(h^2)) + (e^{h\partial_v} + \mathcal{O}(h^2))\}\right]\mathbf{\Psi}(u,v).
\end{aligned} \tag{43}$$

The last expression of Eq. (43) can be expanded immediately, and hence, finally we have

$$\begin{aligned}
\mathbf{\Psi}(u+h,v+h) = \mathbf{\Psi}(u+h,v) + \mathbf{\Psi}(u,v+h) - \mathbf{\Psi}(u,v) \\
- \frac{h^2}{8}\{\mathbf{V}(u+h,v)\mathbf{\Psi}(u+h,v) \\
+ \mathbf{V}(u,v+h)\mathbf{\Psi}(u,v+h)\}.
\end{aligned} \tag{44}$$

This can be thought of as an evolution equation in the light-cone coordinates u and v. The interesting aspect of this formalism is that once initial data are specified in the u, v coordinates, we need no additional boundary conditions, which is unlike the physical coordinates t, r (or, for that matter, t, r_*). We evolve the system with Gaussian initial data in u and constant data in v. Figure 6 illustrates the numerical evolution of Ψ as a function of time for different choices of the angular momenta and Kaluza-Klein mode masses obtained by numerically integrating the above evolution equation in light-cone coordinates. Interestingly and as expected, it illustrates all the basic properties that we have already observed from a quasinormal mode analysis. For example, in all of the cases illustrated in Fig. 6, it is clear that at intermediate times (i.e., when the spectrum of quasinormal modes dominate the evolution of gravitational perturbation) the mode functions due to massive Kaluza-Klein modes will dominate over those in general relativity. This is again due to the fact that the massive modes suffer much less damping compared to the respective ones in general relativity. The translation of the same in the quasinormal mode language corresponds to the imaginary part of the quasinormal mode frequency being smaller for massive Kaluza-Klein modes compared to the modes in general relativity. Further, the fact that as the mass of the Kaluza-Klein mode increases it experiences less and less damping is also borne out by both Cauchy evolution (see Fig. 6) and the quasinormal mode analysis. Of course, there are minute differences present between both of these methods, which have their origin in the initial conditions and the fact that the Cauchy evolution is more accurate compared to the quasinormal mode analysis. All in all, the quasinormal mode analysis and the Cauchy evolution of initial data provide a complete and consistent description of the time evolution of gravitational perturbation in the presence of extra spatial dimensions.

Besides being consistent with the quasinormal mode analysis, Cauchy evolution has more additional features to offer. The most important feature is the presence of the late time power law tail. Since at the intermediate stages, the contributions from the quasinormal mode dominates, the behavior of the mode function $u_{n,l}(t)$ as presented in Fig. 6 resembles those in Section V. However, if one can perform the Cauchy analysis for a sufficiently long time, gradually the contributions from quasinormal modes become smaller compared to that with the late time tail. Thus, the Cauchy evolution of the initial data for a longer time must result in the desired power law tail and will serve as another consistency check of our approach.

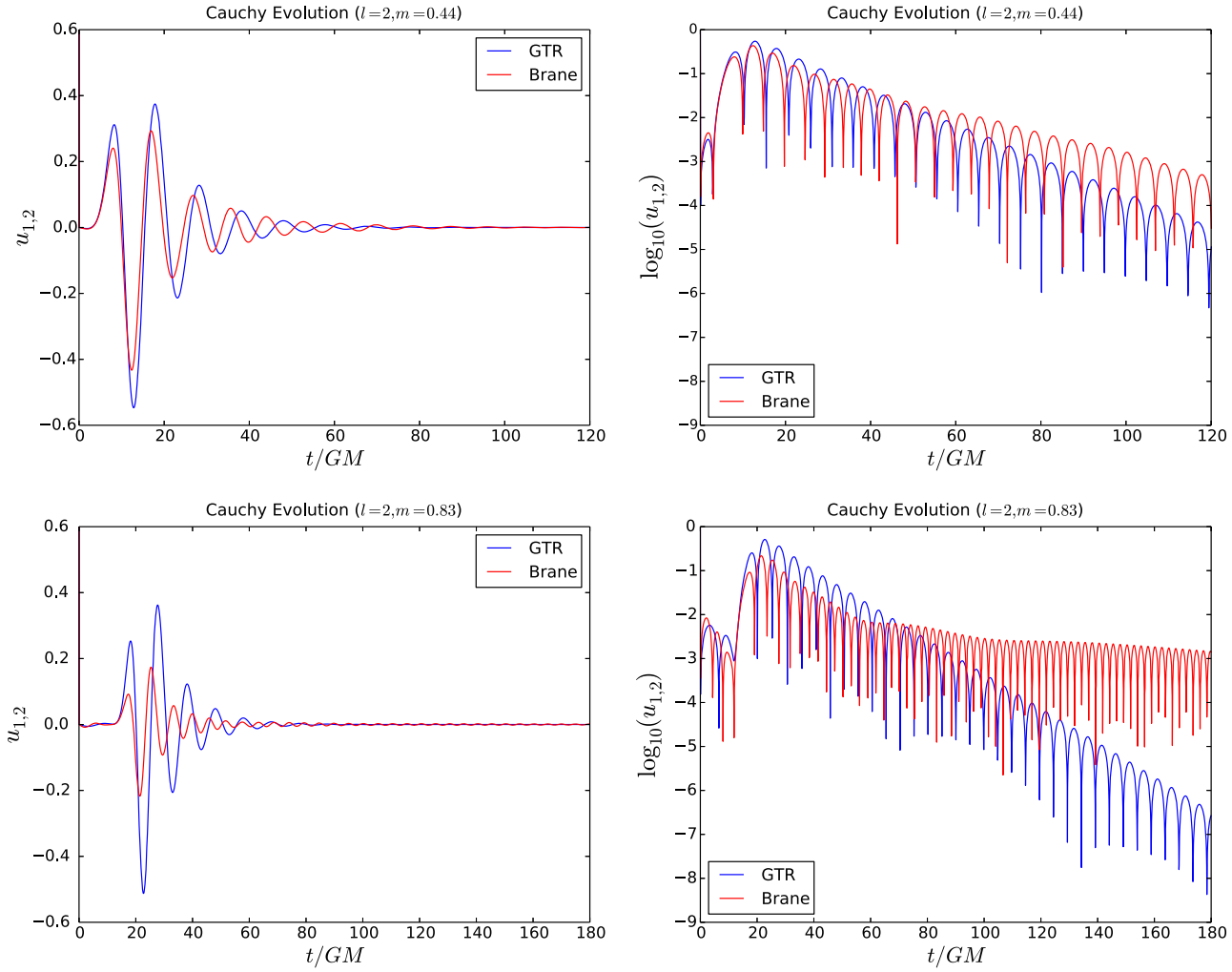

FIG. 6. Cauchy evolution of the master variable $u_{n,l}(t)$ has been plotted for two different choices of the Kaluza-Klein mode masses for a given angular momentum. The figures in the top panel depict the evolution of the master variable for $l = 2$ and $m_1 = 0.44$ and the lowest-lying Kaluza-Klein mode with $d/\ell = 20$ and $1/\ell = 6 \times 10^7$. The figure on the left is the actual variation of the master variable with time, whereas that on the right presents the same variation but in a logarithmic scale. The figures in the bottom panel illustrate the same, however, for $l = 2$ and Kaluza-Klein mode mass $m_2 = 0.83$. It is clear that as the mass increases, the master variable becomes less and less damped in comparison to that with general relativity. Further, we clearly observe that the overall features present in the Cauchy evolution of the master variable are identical to those obtained by the quasinormal mode analysis, illustrating the internal consistency of both the methods adapted here.

Following this, we have presented a long time Cauchy evolution of the perturbation equation in Fig. 7, which distinctly depicts the late time wave tail. As evident from Fig. 7, the mode function is initially dominated by the quasinormal modes and hence decays linearly in the logarithmic scale. However, in the late stages of Cauchy evolution, the power law takes over and dominates the quasinormal modes, thus presenting an almost constant-in-time behavior of the same. Hence, the numerical analysis of the Cauchy evolution of the perturbation equation is completely consistent with theoretical expectation, providing one more consistency check of our formalism.

VII. DISCUSSION AND CONCLUDING REMARKS

In this work, we set out to achieve three goals in a single framework: (a) effect of extra spatial dimensions on the gravitational perturbation and whether one can provide some possible observational signatures of the same in the ringdown phase of black hole merger; (b) how the two possible methods to determine the gravitational perturbation on the brane, namely, by either perturbing the bulk gravitational field equations or perturbing the *effective* gravitational field equations on the brane differ, as far as behavior of the gravitational wave solution is concerned; (c) whether the analysis using quasinormal modes is consistent with the fully numerical Cauchy evolution of

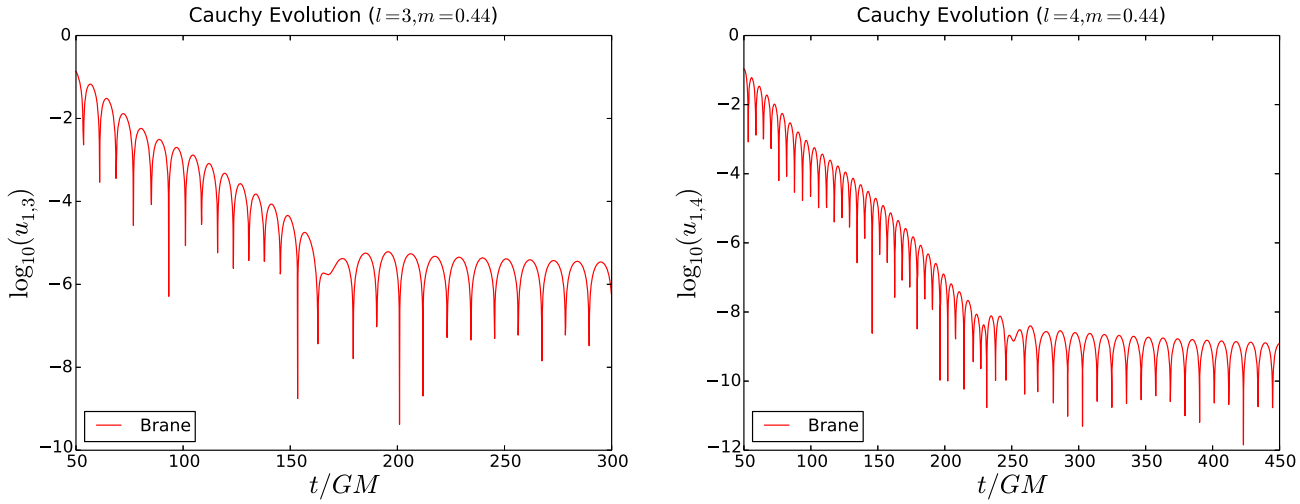

FIG. 7. Cauchy evolution of the master variable $u_{n,l}(t)$ associated with the brane-based approach has been plotted for two different choices of the angular momentum given a Kaluza-Klein mode mass to illustrate the late time behavior. The figure on the left depicts the evolution of the master variable for $l = 3$ and $m_1 = 0.44$ and the lowest-lying Kaluza-Klein mode with $d/\ell = 20$ and $1/\ell = 6 \times 10^7$. The figure on the right is for $l = 4$ and identical Kaluza-Klein mode mass. It is clear that as time progresses, the power law tail dominates over the exponential damping due to quasinormal modes. This once again illustrates the consistency of Cauchy evolution with the theoretical methods adapted here.

the initial data. We believe to have addressed all of them in a satisfactory manner in this work, which we summarize below.

We have explicitly demonstrated that the existence of extra spatial dimensions indeed modifies the gravitational perturbation equation by essentially introducing a tower of massive perturbation modes in addition to the standard massless one. Thus, the presence of massive gravitational perturbation modes is a definitive signature of the existence of higher dimensions. To see the consequences of the above, we have discussed the behavior of quasinormal modes in this context. In particular, we have shown that for the massive modes, the imaginary parts of the quasinormal mode frequencies are much smaller compared to those in general relativity. This has resulted in the time evolution of the massive gravitational perturbations exhibiting a weak decay rate in comparison to the massless modes as in general relativity. The above phenomenon opens up the observational window to probe the possible existence of higher dimensions using gravitational wave observation. If the ringdown phase during the merger of two black holes is loud enough to be accurately measured for a sufficient amount of time (unlike the aLIGO-VIRGO observations to-date) it may be possible to detect any departure from the general relativity prediction, and thus may lead to a concrete observational signature for the existence of higher dimensions, or may provide stringent constraints on the associated parameters. This will become feasible as the sensitivity of the aLIGO detectors is further improved or the space-based gravitational wave detector LISA becomes operational. We will address the detailed observational aspects of this particular signature of extra dimensions in light of the recent detection of gravitational waves at aLIGO in a future work.

The evolution equation for the gravitational perturbation obtained by perturbing the bulk field equations has already been derived in [68], whereas in this work, we have derived the evolution equation by perturbing the *effective* gravitational field equations on the brane hypersurface. From the structure of the equation itself, the difference between these two approaches should be evident. In both the bulk-based and the brane-based approaches, the four-dimensional perturbation equation looks identical with one crucial difference, namely, the masses associated with both approaches are different. This is because the differential equation satisfied by the extra-dimensional part is different in these two scenarios. This, in turn, leads to the difference in the quasinormal mode frequencies as evident from Fig. 1, and the imaginary parts of the quasinormal mode frequencies for the bulk-based approach are smaller than those for the brane-based one. Because the difference is small, there is possibly no way in the foreseeable future to observationally distinguish these two effects (see, e.g., Fig. 5); however, theoretically, there does exist a difference between these approaches. Naively speaking, this is due to the fact that a solution of the *effective* gravitational field equation on the brane may not have any higher-dimensional embedding.

Finally, the time evolution of the gravitational perturbation can be obtained by either performing a quasinormal mode analysis or by performing a fully numerical Cauchy evolution. We have performed both in this work, and they are found to match very well with each other. This is expected as well as necessary for internal consistency of

any gravitational perturbation computation. In particular, from the quasinormal mode analysis, we have learned that the massive modes decay very slowly, in contrast with the massless general relativity modes (see, e.g., Fig. 3), which is also confirmed by the Cauchy evolution (see, e.g., Fig. 6). Thus keeping aside minute details, overall behavior of the time evolution of gravitational perturbation is identical whether one performs a quasinormal mode analysis or complete Cauchy evolution.

Having described the consistency of the time evolution obtained by using quasinormal modes as well as a fully numerical Cauchy evolution of the perturbation equations, let us comment on possible detectability of the scenario presented above. For that purpose, it is important to know the frequencies associated with the gravitational perturbation modes. The corresponding frequencies can broadly be divided into two classes, those originating from the real part of the quasinormal modes of the gravitational perturbation and the universal one present in the very late time region [68,103] originating from the power law tail. As far as the possible detectability of the scenario presented here in aLIGO-like detectors using the real parts of the quasinormal modes is concerned, one can safely say that most likely it is not a feasible option. This is mainly due to two reasons. First, the frequencies associated with these Kaluza-Klein modes are smaller compared to those with general relativity (see Table VII as well as Fig. 8). Furthermore, these Kaluza-Klein modes are supposed to be excited in the strong gravity regime, i.e., when mass of the black hole is large. On the other hand, as the mass of the black hole increases, the frequency also decreases. This adds to the issue of detectability of these Kaluza-Klein modes. As evident from Table VII, for black hole mass $\sim 10^3\ M_\odot$, the frequency of a mode in general relativity is within the frequency band of aLIGO detectors. However, the same is not true for the Kaluza-Klein modes where the frequencies are smaller and hence possibly outside the operational band of the aLIGO detectors. Nonetheless, all of these frequencies pertaining to higher mass black holes are very well within the projected frequency band of LISA and hence possibly detectable in the near future (see Fig. 8). The second point corresponds to the signal-to-noise ratio because, in order to detect the signal, it is necessary to generate oscillations with a high signal-to-noise ratio. For this purpose, as well, we need collisions among heavier black holes (i.e., stronger gravity regime), so that higher-order massive KK modes are excited. The frequency of these modes would correspondingly be lower and might get

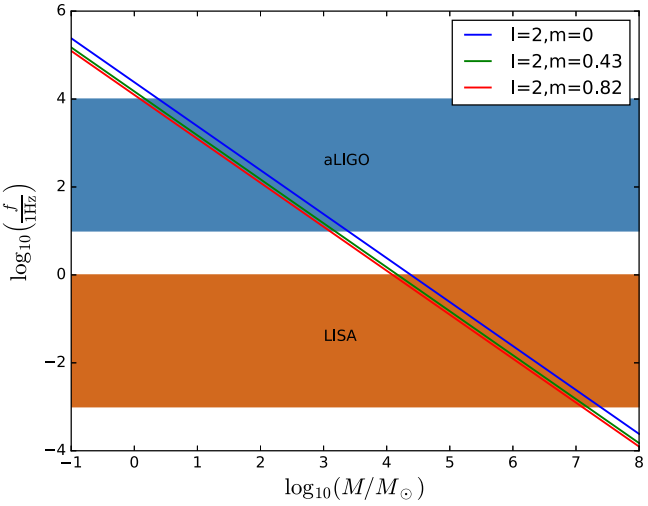

FIG. 8. This figure depicts how the oscillation frequency of the gravitational wave in the ringdown phase changes as the mass of the black hole increases. For convenience, frequencies are plotted in Hz, and black hole mass is presented in solar units, but both on a logarithmic scale. The oscillation frequencies have been plotted in the brane-based scenarios for two lowest-lying Kaluza-Klein mode masses with $l = 2$. The same has been contrasted with the corresponding curve in general relativity. It is clear that for $M \sim 10^3\ M_\odot$, the frequencies associated with general relativity are well within the aLIGO frequency band; however, for the massive Kaluza-Klein modes they are outside. Because these massive modes have a better chance of getting detected in the high mass regime, it is most likely that they may become observable once LISA is operational. See text for more discussions.

TABLE VII. Frequencies (in Hz) of oscillation for the quasinormal modes emanating from black holes having different masses have been depicted. Numerical estimates for the frequencies have been presented for general relativity as well as for the two lowest lying Kaluza-Klein modes with masses $m_1 = 0.43$ and $m_2 = 0.83$ respectively. It is also clear that the frequency of the modes increases with an increase in the l value. It is clear that as the mass of the black hole increases the frequency decreases. Thus more massive the black hole is it is more problematic to detect in aLIGO. While the Kaluza-Klein modes have better chance of originating if the mass of the black hole increases, this leads to lowering of the frequency and hence have less chance of getting detected in aLIGO.

Frequencies for $l = 2$			
$(M/M_\odot)$	General Relativity	KK Mode ($m_1 = 0.43$)	KK Mode ($m_2 = 0.82$)
1	24140	14930	12441
10	2414	1493	1244.1
10^2	241.4	149.3	124.4
10^3	24.1	14.9	12.4
10^4	2.4	1.5	1.2
10^5	0.2	0.1	0.1
Frequencies for $l = 3$			
1	38779	21328	27856
10	3877.9	2132.8	2785.6
10^2	387.7	213.3	278.6
10^3	38.7	21.3	27.8
10^4	3.9	2.1	2.8
10^5	0.3	0.2	0.3

pushed out of the aLIGO frequency band but possibly be well within the LISA band.

The late time behavior of these massive gravitational perturbation modes corresponds to a universal frequency, associated with the power law tail of the wave mode and proportional to the Kaluza-Klein mode mass [68,103]. Thus, the frequency is determined in terms of the d/ℓ ratio and the curvature length scale ℓ. Using the expression for nth Kaluza-Klein mode mass, $m_n = z_n(1/\ell)\exp(d/\ell)$, where z_n are the zeros of the Bessel function $J_{\sqrt{13}/2}(x)$, one immediately arrives at the desired expression for the late time frequency as a function of d/ℓ and $1/\ell$. Given this universal late time frequency, one immediately observes that as d/ℓ and $1/\ell$ increase, the frequency also increases, and hence for a given d/ℓ ratio, the frequency will be in the aLIGO band for a larger value of $1/\ell$ but will fall within the LISA band for smaller values of $1/\ell$ (as evident from Fig. 9). This introduces additional complications in the detectability of these late time mode modulo of the Gregory-Laflamme instability, which sets in for small $1/\ell$ values given a d/ℓ (see Fig. 9). At this point, it is interesting to note that, given a black hole mass and a particular value of ℓ, the frequency bands of aLIGO and LISA set natural observational bounds on d/ℓ. In Fig. 9, we have considered two such scenarios, where the black hole masses are 50 $M_\odot$ and 10^5 $M_\odot$, with $\ell = 1$ μm. The scenarios are depicted by the thick green and blue lines, respectively. As is clearly evident from the plot, the modes from the 50 $M_\odot$ black hole can probe the range $17.0 < d/\ell < 23.9$. The 10^5 $M_\odot$ black hole has only a limited probe for d/ℓ because of the unstable configurations. The upper limit on d/ℓ in this case is therefore set by the boundary of the unstable region, so that $33.8 < d/\ell < 34.8$. Thus, as long as the universal frequency spectrum is concerned, the late time behavior of the Kaluza-Klein modes has a better chance of detection in aLIGO rather than in LISA, as clearly depicted in Fig. 9. The feasibility of the above detection, however, is being determined by the signal-to-noise ratio, which will be much less for aLIGO but will be favorable for LISA. Hence, even in this case, there will be a tussle between the accessible regions in the $(d/\ell, 1/\ell)$ space and the signal-to-noise ratio, making the detectability difficult for aLIGO detectors for the late time behavior of the massive quasinormal modes, as well.

The above exercise also opens up a few future avenues to explore. We have discussed the effect of higher dimensions on the quasinormal modes in this work; however, it is possible to address the nature of quasibound states and, in particular, how the presence of extra dimensions affect them. This may provide another observational test bed for detection of higher spatial dimensions. Whether one can obtain similar results for the quasibound states from Cauchy evolution, as well, remains to be verified. Also, a thorough analysis of this allowed region in light of the recent detection of gravitational waves in aLIGO can lead to possible constraints on the extra-dimensional parameter space. Moreover, the effect of higher dimensions on the neutron star equation of state parameter, tidal love numbers associated with a brane black hole can lead to exciting results, which we are currently pursuing and will report elsewhere.

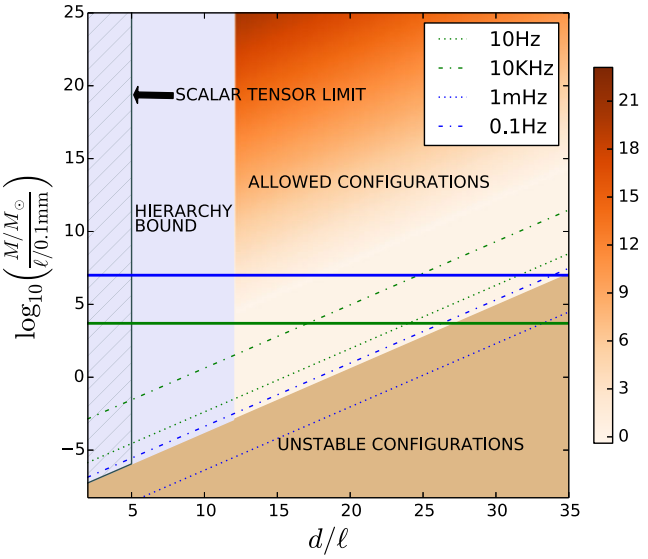

FIG. 9. This figure depicts the allowed region in the $(d/\ell, M/\ell)$ plane along with the frequency associated with the very late time behavior of the perturbation modes for black holes. The accessible region in the plot is obtained by imposing a few restrictions on the d/ℓ as well as M/ℓ values. These correspond to (a) the Gregory-Laflamme instability, (b) the scalar-tensor limit, and finally (c) the restriction on d/ℓ necessary to solve the hierarchy problem. The frequencies of the late time behavior of the perturbation modes have been depicted in the accessible region by means of a color coding. The labels on the right hand color bar correspond to a logarithm of frequencies (in Hz) to the base 10. The green-dotted and dash-dotted lines correspond to frequencies of 10 Hz and 10 KHz, respectively, the extremities of the aLIGO band. Similarly, the blue broken lines correspond to the extremities of the LISA band. The solid green and blue lines correspond to a configuration with $\ell = 1/4$ μm and M of 50 $M_\odot$ and 10^5 $M_\odot$, respectively. For a given d/ℓ ratio as $1/\ell$ increases, the frequency also increases, whereas for a given $1/\ell$, as d/ℓ increases, the frequency decreases. Hence, the aLIGO band is completely within the accessible region, and the LISA band has substantial overlap with the unstable regions. See text for more discussions.

ACKNOWLEDGMENTS

Research of S. C. is supported by the SERB-NPDF Grant No. (PDF/2016/001589) from SERB, Government of India, and the research of S. S.G is partially supported by the SERB-Extra Mural Research Grant No. (EMR/2017/001372), Government of India. This work was supported in part by NSF Grant No. PHY-1506497 and the Navajbai Ratan Tata Trust. The authors gratefully acknowledge

discussions with David Hilditch, Emanuele Berti, Paolo Pani, and Sanjeev Seahra. We also thank Shasvath Kapadia for carefully reading the manuscript and making useful suggestions. This work has been assigned the LIGO document number LIGO-P1700295.

APPENDIX A: DERIVING THE PERTURBED GRAVITATIONAL FIELD EQUATIONS ON THE BRANE

In this appendix, we present the detailed derivation of the perturbed gravitational field equations on the brane for completeness. We start with various geometrical quantities associated with spacetime curvature and express their perturbative expansion to leading order in h_{AB}. These correspond to

$$R^{(h)}_{ABCD} = \frac{1}{2}\{\nabla_C\nabla_D h_{AB} + \nabla_C\nabla_B h_{AD} - \nabla_C\nabla_A h_{BD} - \nabla_D\nabla_C h_{AB} - \nabla_D\nabla_B h_{AC} + \nabla_D\nabla_A h_{BC}\}, \quad \text{(A1)}$$

$$R^{(h)}_{AB} = \frac{1}{2}\{-\nabla_C\nabla^C h_{AB} - 2h^C_D R^{(g)D}_{\ \ ACB} + h^D_A R^{(g)}_{DB} + h^D_B R^{(g)}_{DA}\}, \quad \text{(A2)}$$

$$R^{(h)} = \nabla_C\nabla_B h^{CB} - \nabla_C\nabla^C h = 0. \quad \text{(A3)}$$

In order to arrive at the last line, the gauge conditions introduced in Eq. (5) have been used. These gauge conditions further enable one to arrive at the following result:

$$\nabla_C\nabla_B h^C_A - \nabla_B\nabla_C h^C_A = h^D_A R^{(g)}_{DB} - h^C_D R^{(g)D}_{\ \ ACB}, \quad \text{(A4)}$$

which has also been used in deriving Eq. (A2). As we are ultimately interested in perturbation equations on the brane, it is instructive to rewrite all the bulk quantities in terms of brane variables. In particular, conversion of the bulk covariant derivatives to the brane covariant derivative is a necessary and important step in that direction because these are the terms appearing in Eqs. (A1), (A2), and (A3). This can be done by elaborating all of the bulk covariant derivatives into ordinary derivatives and Christoffel connections and then picking up all the terms involving brane covariant derivatives as well as terms depending on the bulk curvature and derivative with respect to y. Further, as $x^A = (y, x^\mu)$, it is clear that $e^A_\mu = \delta^A_\mu$. Thus, we obtain from Eq. (A1)

$$\begin{aligned} 2R^{(h)}_{ABCD}e^A_\mu n^B e^C_\nu n^D &= 2\nabla_\nu\nabla_y h_{\mu y} - \nabla_\nu\nabla_\mu h_{yy} - \nabla_y\nabla_\nu h_{\mu y} - \nabla_y\nabla_y h_{\mu\nu} + \nabla_y\nabla_\mu h_{y\nu} \\ &= -\partial_y^2 h_{\mu\nu} - 2k\partial_y h_{\mu\nu}. \end{aligned} \quad \text{(A5)}$$

Two other contractions in Eq. (10) involving the perturbed Ricci tensor $R^{(h)}_{AB}$ result in

$$\begin{aligned} R^{(h)}_{AC}e^A_\mu e^C_\nu &= -\frac{1}{2}\nabla_C\nabla^C h_{\mu\nu} - h^\alpha_\beta R^{(g)\beta}_{\ \ \mu\alpha\nu} + \frac{1}{2}h^\alpha_\mu R^{(g)}_{\alpha\nu} + \frac{1}{2}h^\alpha_\nu R^{(g)}_{\alpha\mu} \\ &= -\frac{1}{2}{}^{(4)}\Box h_{\mu\nu} - \frac{1}{2}\partial_y^2 h_{\mu\nu} + 3k^2 h_{\mu\nu} - h^\alpha_\beta R^{(g)\beta}_{\ \ \mu\alpha\nu} + \frac{1}{2}h^\alpha_\mu R^{(g)}_{\alpha\nu} + \frac{1}{2}h^\alpha_\nu R^{(g)}_{\alpha\mu}, \end{aligned} \quad \text{(A6)}$$

and

$$R^{(h)}_{AC}n^A n^C = -\frac{1}{2}\nabla_C\nabla^C h_{yy} - h^\alpha_\beta R^{(g)\beta}_{\ \ y\alpha y} = -h^\alpha_\beta R^{(g)\beta}_{\ \ y\alpha y}, \quad \text{(A7)}$$

where Eq. (A2) has been used. In order to arrive at the previous expressions, the gauge conditions presented in Eq. (5) have been used along with the following set of results:

$$\begin{aligned} g^{CD}\nabla_C\nabla_D h_{\alpha\beta} &= {}^{(4)}\Box h_{\alpha\beta} + \partial_y^2 h_{\alpha\beta} - 6k^2 h_{\alpha\beta} \\ \nabla_\nu\nabla_y h_{\mu y} &= k\partial_y h_{\mu\nu} + 3k^2 h_{\mu\nu} \\ -\nabla_\nu\nabla_\mu h_{yy} &= -2k^2 h_{\mu\nu} \\ -\nabla_y\nabla_\nu h_{y\mu} &= -k\partial_y h_{\mu\nu} - 2k^2 h_{\mu\nu} \\ -\nabla_y\nabla_y h_{\mu\nu} &= -\partial_y^2 h_{\mu\nu} - 4k\partial_y h_{\mu\nu} - 4k^2 h_{\mu\nu} \\ \nabla_y\nabla_\mu h_{y\nu} &= k\partial_y h_{\mu\nu} + 2k^2 h_{\mu\nu}. \end{aligned} \quad \text{(A8)}$$

In arriving at the above relation, we have also used the conditions that there exist only two nonvanishing connection components having the following forms: $\Gamma^y_{\mu\nu} = kq_{\mu\nu}$ and $\Gamma^\mu_{y\nu} = -k\delta^\mu_\nu$. Use of these expressions for various projections of Riemann and Ricci tensor from Eqs. (A5), (A6), and (A7) in the perturbation equation for the bulk Weyl tensor as in Eq. (10) leads to

$$\begin{aligned} E^{(h)}_{\mu\nu} &= \frac{1}{2}(-\partial_y^2 h_{\mu\nu} - 2k\partial_y h_{\mu\nu}) - \frac{1}{3}q_{\mu\nu}(-h^\alpha_\beta R^{(g)\beta}_{\ \ y\alpha y}) - \frac{1}{3}h_{\mu\nu}R^{(g)}_{yy} + \frac{1}{12}R^{(g)}h_{\mu\nu} \\ &\quad - \frac{1}{3}\left(-\frac{1}{2}{}^{(4)}\Box h_{\mu\nu} - \frac{1}{2}\partial_y^2 h_{\mu\nu} + 3k^2 h_{\mu\nu} - h^{\alpha\beta}R^{(g)\beta}_{\ \ \mu\alpha\nu} + \frac{1}{2}h^\alpha_\mu R^{(g)}_{\alpha\nu} + \frac{1}{2}h^\alpha_\nu R^{(g)}_{\alpha\mu}\right). \end{aligned} \quad \text{(A9)}$$

It is obvious that, in order to separate out the perturbation of the bulk Weyl tensor into a four-dimensional part and an additional part originating from extra dimensions, one needs to decompose all the quantities depending on the bulk metric g_{AB} in terms of the four-dimensional metric $q_{\alpha\beta}$. For that purpose, we consider the following decompositions:

$$R^{(g)\beta}_{\mu\alpha\nu} = {}^{(4)}R^{(q)\beta}_{\mu\alpha\nu} - k^2(q_{\mu\nu}\delta^\beta_\alpha - q_{\mu\alpha}\delta^\beta_\nu)$$
$$R^{(g)\beta}_{y\alpha y} = -k^2\delta^\beta_\alpha, \tag{A10}$$

$$R^{(g)}_{\alpha\mu} = {}^{(4)}R^{(q)}_{\alpha\mu} - 4k^2 q_{\alpha\mu}$$
$$R^{(g)}_{yy} = -4k^2; \qquad R^{(g)} = {}^{(4)}R^{(q)} - 20k^2. \tag{A11}$$

This eventually results in (11).

APPENDIX B: CONTINUED FRACTION METHOD: DETAILED ANALYSIS

In this appendix, we provide a detailed and general derivation of the three-term recursion relation pertaining to the continued fraction method, which we hope will be useful for the reader. Having derived Eqs. (32) and (33), one normally makes an educated guess for $\psi_{n,l}$ and $\phi_{n,l}$, respectively. However, as we will explicitly demonstrate, this is not necessary. One can start with an arbitrary choice for $\psi_{n,l}$ and $\phi_{n,l}$, but the structure of the differential equation itself will lead to the correct expressions for the master variables. Following this philosophy, we decompose $\psi_{n,l}$ and $\phi_{n,l}$ as follows:

$$\psi_{n,l} = (r-2)^\alpha r^\beta \exp(\lambda r) f_{n,l}(r), \tag{B1}$$

$$\phi_{n,l} = (r-2)^\alpha r^\beta \exp(\lambda r) g_{n,l}(r), \tag{B2}$$

where α, β, and λ are arbitrary constants appearing in the master variables which we would like to uniquely determine using the structure of the differential equation. Substitution of these forms in Eqs. (32) and (33) yields the following differential equations for $f_{n,l}$ and $g_{n,l}$ respectively:

$$r(r-2)\frac{d^2 f_{n,l}(r)}{dr^2} + \{2\lambda r^2 + (2\alpha + 2\beta - 4\lambda)r + (2 - 4\beta)\}\frac{df_{n,l}(r)}{dr}$$
$$+ \{(\lambda^2 - m_n^2)r^2 + (-2\lambda^2 + 2\alpha\lambda + 2\beta\lambda)r + \frac{\omega^2 r^3 + 2\alpha^2}{r-2} - \frac{2\beta^2 - 4\beta - 6}{r}$$
$$+ (2\lambda - 4\beta\lambda + \beta(\beta-1) + \alpha(\alpha-1) - l(l+1) + 2\alpha\beta)\}f_{n,l}(r) - \frac{m_n^2}{r} g_{n,l} = 0, \tag{B3}$$

$$r(r-2)\frac{d^2 g_{n,l}(r)}{dr^2} + \{2\lambda r^2 + (2\alpha + 2\beta - 4\lambda)r + (2 - 4\beta)\}\frac{dg_{n,l}(r)}{dr}$$
$$+ \{(\lambda^2 - m_n^2)r^2 + (-2\lambda^2 + 2\alpha\lambda + 2\beta\lambda)r + \frac{\omega^2 r^3 + 2\alpha^2}{r-2} - \frac{2\beta^2 - 4\beta}{r}$$
$$+ (2\lambda - 4\beta\lambda + \beta(\beta-1) + \alpha(\alpha-1) - l(l+1) + 2\alpha\beta)\}f_{n,l}(r) - 4 f_{n,l} = 0. \tag{B4}$$

Given these differential equations, one changes the variable from r to ξ, such that $r = 2/(1-\xi)$. In order for these differential equations to have regular singular points after the variable change, it is necessary that the terms behaving as r^2, r, and $1/(r-2)$ in the above should vanish, which would require, at the first level, $\alpha = -2i\omega$, in which case one can use the following relation, $r^3 - 8 = (r-2)(r^2 + 2r + 4)$, such that the other two parameters λ and β are determined as $\lambda = \sqrt{m_n^2 - \omega^2}$ and $\beta = 2i\omega + (1/\lambda)(-\omega^2 + \lambda^2) = -(1/\lambda)(\omega - i\lambda)^2$. Hence, the substitutions of these three constants leads to the following ansatz for the master variable suited with the above problem,

$$\psi_{n,l} = \left(\frac{r-2}{r}\right)^{-2i\omega} r^{-b} e^{\lambda r} f_{n,l},$$
$$\lambda = \sqrt{m_n^2 - \omega^2}; \qquad b = \frac{\omega^2 - \lambda^2}{\lambda}, \tag{B5}$$

$$\phi_{n,l} = \left(\frac{r-2}{r}\right)^{-2i\omega} r^{-b} e^{\lambda r} g_{n,l}. \tag{B6}$$

Using Eqs. (B5) and (B6), both the differential equations can be casted in the following form:

$$r(r-2)\frac{d^2 y}{dr^2} + \{Ar^2 + Br + C\}\frac{dy}{dr}$$
$$+ \left\{D + \frac{E}{r}\right\}y + \left\{F + \frac{G}{r}\right\}z = 0, \tag{B7}$$

where y stands for $f_{n,l}$ and z stands for $g_{n,l}$ or vice versa, and the constants appearing in the above differential equation will depend on the parameters introduced above in Eqs. (B5) and (B6). As mentioned earlier, it is advantageous to introduce a new variable, $\xi = (r-2)/r$, in lieu of r, such that $r = 2/(1-\xi)$. Eliminating the variable r appearing in Eq. (B7), one can rewrite the differential equation in terms of the new variable ξ. Simplifying the resulting differential equation further, we obtain

$$\xi(1-\xi)^2\frac{d^2y}{d\xi^2}+\left\{\left(2A+B+\frac{C}{2}\right)-(2+B+C)\xi+\left(2+\frac{C}{2}\right)\xi^2\right\}\frac{dy}{d\xi}+\left\{\left(D+\frac{E}{2}\right)-\frac{E}{2}\xi\right\}y+\left\{\left(F+\frac{G}{2}\right)-\frac{G}{2}\xi\right\}z=0. \tag{B8}$$

The above differential equation can be solved using the power series technique. Keeping this in mind, let us assume the following series expansion for y in powers of $(r-2)/r$ or in terms of ξ as

$$y\equiv\sum_{j=0}c_j\left(\frac{r-2}{r}\right)^j=\sum_{j=0}c_j\xi^j;\qquad z=\sum_{j=0}d_j\xi^j, \tag{B9}$$

where c_j and d_j are arbitrary coefficients that need to be determined. Substitution of the above power series in the differential equation given by Eq. (B8) results in an equation involving various powers of ξ. Simplifying the above algebraic equation further and writing it in such a manner that all the powers of ξ coincide, we finally obtain the following three-term recursion relation between three coefficients c_{j-1}, c_j, and c_{j+1} as well as d_j and d_{j-1} appearing in the series expansion in Eq. (B9) as

$$(j+1)\left(j+2A+B+\frac{C}{2}\right)c_{j+1}-\left\{2j(j-1)+n(2+B+C)-\left(D+\frac{E}{2}\right)\right\}c_j+\left\{(j-1)(j-2)+\left(2+\frac{C}{2}\right)(j-1)-\frac{E}{2}\right\}c_{j-1}+d_j\left(F+\frac{G}{2}\right)-\frac{G}{2}d_{j-1}=0. \tag{B10}$$

As we have mentioned earlier, the same recursion relation holds for expansion coefficients of $f_{n,l}$ and $g_{n,l}$, but the constants appearing in the recursion relation will have distinct values for the two situations. In the case of $f_{n,l}$, we have the following expressions for the constants:

$$\begin{aligned}&A=2\lambda;\qquad B=2\alpha+2\beta-4\lambda,\\&C=2-4\beta;\qquad E=-2\beta^2+4\beta+6,\\&D=2\lambda-4\beta\lambda+\beta(\beta-1)+\alpha(\alpha-1)\\&\qquad-l(l+1)+2\alpha\beta+4\omega^2,\\&F=0;\qquad G=-m_n^2,\end{aligned} \tag{B11}$$

where the corresponding values associated with the differential equation for $g_{n,l}$ become

$$\begin{aligned}&A=2\lambda;\qquad B=2\alpha+2\beta-4\lambda,\\&C=2-4\beta;\qquad E=-2\beta^2+4\beta,\\&D=2\lambda-4\beta\lambda+\beta(\beta-1)+\alpha(\alpha-1)\\&\qquad-l(l+1)+2\alpha\beta+4\omega^2,\\&F=-4;\qquad G=0.\end{aligned} \tag{B12}$$

Using these constants, one can write down the three-term recursion relation for both the master variables, which we have used to arrive at Eq. (34).

[1] A. Perez-Lorenzana, An Introduction to extra dimensions, J. Phys. Conf. Ser. **18**, 224 (2005).

[2] C. Csaki, TASI lectures on extra dimensions and branes, in *From fields to strings: Circumnavigating theoretical physics. Ian Kogan memorial collection (3 volume set)* (World Scientific, Singapore, 2004) pp. 605–698.

[3] R. Sundrum, Tasi 2004 lectures: To the fifth dimension and back, in *Theoretical Advanced Study Institute in Elementary Particle Physics: Many Dimensions of String Theory (TASI 2005), Boulder, Colorado, June 5-July 1, 2005*, pp. 585–630 2005.

[4] J. Polchinski, *String Theory. An Introduction to the Bosonic String*, Vol. 1 (Cambridge University Press, Cambridge, England, 1998).

[5] J. Polchinski, *String Theory. Superstring Theory and Beyond*, Vol. 2 (Cambridge University Press, Cambridge, England, 1998).

[6] C. Rovelli, *Quantum gravity* (Cambridge University Press, Cambridge, England, 2004).

[7] S. Chakraborty, *Classical and quantum aspects of gravity in relation to the emergent paradigm* (Springer, New York, 2017).

[8] N. Arkani-Hamed, S. Dimopoulos, and G. Dvali, The Hierarchy problem and new dimensions at a millimeter, Phys. Lett. B **429**, 263 (1998).

[9] I. Antoniadis, N. Arkani-Hamed, S. Dimopoulos, and G. Dvali, New dimensions at a millimeter to a Fermi and superstrings at a TeV, Phys. Lett. B **436**, 257 (1998).

[10] I. Antoniadis, A Possible new dimension at a few TeV, Phys. Lett. B **246**, 377 (1990).
[11] V. Rubakov and M. Shaposhnikov, Extra space-time dimensions: Towards a solution to the cosmological constant problem, Phys. Lett. **125B**, 139 (1983).
[12] V. Rubakov and M. Shaposhnikov, Do we live inside a domain wall?, Phys. Lett. B **125**, 136 (1983).
[13] L. Randall and R. Sundrum, A Large mass hierarchy from a small extra dimension, Phys. Rev. Lett. **83**, 3370 (1999).
[14] J. Garriga and T. Tanaka, Gravity in the brane world, Phys. Rev. Lett. **84**, 2778 (2000).
[15] A. Chamblin, S. Hawking, and H. Reall, Brane world black holes, Phys. Rev. D **61**, 065007 (2000).
[16] E. Berti *et al.*, Testing general relativity with present and future astrophysical observations, Classical Quantum Gravity **32**, 243001 (2015).
[17] R. A. Konoplya and A. Zhidenko, (In)stability of D-dimensional black holes in Gauss-Bonnet theory, Phys. Rev. D **77**, 104004 (2008).
[18] R. A. Konoplya and A. Zhidenko, Stability of multidimensional black holes: Complete numerical analysis, Nucl. Phys. **B777**, 182 (2007).
[19] E. Berti, V. Cardoso, and A. O. Starinets, Quasinormal modes of black holes and black branes, Classical Quantum Gravity **26**, 163001 (2009).
[20] R. Gregory, Braneworld black holes, Lect. Notes Phys. **769**, 259 (2009).
[21] R. Emparan, G. T. Horowitz, and R. C. Myers, Exact description of black holes on branes, J. High Energy Phys. 01 (2000) 007.
[22] W. G. Cook, U. Sperhake, E. Berti, and V. Cardoso, Black-hole head-on collisions in higher dimensions, Phys. Rev. D **96**, 124006 (2017).
[23] C. Csaki, M. Graesser, L. Randall, and J. Terning, Cosmology of brane models with radion stabilization, Phys. Rev. D **62**, 045015 (2000).
[24] C. Csaki, M. Graesser, C. F. Kolda, and J. Terning, Cosmology of one extra dimension with localized gravity, Phys. Lett. B **462**, 34 (1999).
[25] P. Binetruy, C. Deffayet, and D. Langlois, Nonconventional cosmology from a brane universe, Nucl. Phys. **B565**, 269 (2000).
[26] D. Ida, Brane world cosmology, J. High Energy Phys. 09 (2000) 014.
[27] S. Nojiri, S. D. Odintsov, and S. Ogushi, Cosmological and black hole brane world universes in higher derivative gravity, Phys. Rev. D **65**, 023521 (2001).
[28] S. Nojiri, S. D. Odintsov, and S. Ogushi, Friedmann-Robertson-Walker brane cosmological equations from the five-dimensional bulk (A)dS black hole, Int. J. Mod. Phys. A **17**, 4809 (2002).
[29] C. Charmousis and J.-F. Dufaux, General Gauss-Bonnet brane cosmology, Classical Quantum Gravity **19**, 4671 (2002).
[30] C. Germani and C. F. Sopuerta, String inspired brane world cosmology, Phys. Rev. Lett. **88**, 231101 (2002).
[31] E. Gravanis and S. Willison, Israel conditions for the Gauss-Bonnet theory and the Friedmann equation on the brane universe, Phys. Lett. B **562**, 118 (2003).
[32] P. Brax, C. van de Bruck, and A.-C. Davis, Brane world cosmology, Rep. Prog. Phys. **67**, 2183 (2004).
[33] W. D. Goldberger and M. B. Wise, Phenomenology of a stabilized modulus, Phys. Lett. B **475**, 275 (2000).
[34] H. Davoudiasl, J. Hewett, and T. Rizzo, Bulk gauge fields in the Randall-Sundrum model, Phys. Lett. B **473**, 43 (2000).
[35] H. Davoudiasl, J. Hewett, and T. Rizzo, Experimental probes of localized gravity: On and off the wall, Phys. Rev. D **63**, 075004 (2001).
[36] W. D. Goldberger and M. B. Wise, Modulus stabilization with bulk fields, Phys. Rev. Lett. **83**, 4922 (1999).
[37] Z. Chacko and A. E. Nelson, A solution to the hierarchy problem with an infinitely large extra dimension and moduli stabilization, Phys. Rev. D **62**, 085006 (2000).
[38] S. Chakraborty and S. SenGupta, Higher curvature gravity at the LHC, Phys. Rev. D **90**, 047901 (2014).
[39] S. Chakraborty and S. Sengupta, Radion cosmology and stabilization, Eur. Phys. J. C **74**, 3045 (2014).
[40] S. Chakraborty and S. SenGupta, Gravity stabilizes itself, Eur. Phys. J. C **77**, 573 (2017).
[41] I. Banerjee, S. Chakraborty, and S. SenGupta, Excavating black hole continuum spectrum: Possible signatures of scalar hairs and of higher dimensions, Phys. Rev. D **96**, 084035 (2017).
[42] S. Chakraborty and S. SenGupta, Strong gravitational lensing—A probe for extra dimensions and Kalb-Ramond field, J. Cosmol. Astropart. Phys. 07 (2017) 045.
[43] B. P. Abbott *et al.* Virgo, LIGO Scientific Collaborations, GW170104: Observation of a 50-Solar-Mass Binary Black Hole Coalescence at Redshift 0.2, Phys. Rev. Lett. **118**, 221101 (2017).
[44] B. P. Abbott *et al.* Virgo, LIGO Scientific Collaborations, Binary Black Hole Mergers in the first Advanced LIGO Observing Run, Phys. Rev. X **6**, 041015 (2016).
[45] B. P. Abbott *et al.* Virgo, LIGO Scientific Collaborations, GW151226: Observation of Gravitational Waves from a 22-Solar-Mass Binary Black Hole Coalescence, Phys. Rev. Lett. **116**, 241103 (2016).
[46] B. P. Abbott *et al.* Virgo, LIGO Scientific Collaboration, Tests of general relativity with GW150914, Phys. Rev. Lett. **116**, 221101 (2016).
[47] B. P. Abbott *et al.* Virgo, LIGO Scientific Collaboration, Observation of Gravitational Waves from a Binary Black Hole Merger, Phys. Rev. Lett. **116**, 061102 (2016).
[48] H. Asada, M. Shibata, and T. Futamase, PostNewtonian hydrodynamic equations using the $(3+1)$ formalism in general relativity, Prog. Theor. Phys. **96**, 81 (1996).
[49] T. Damour, P. Jaranowski, and G. Schaefer, Effective one body approach to the dynamics of two spinning black holes with next-to-leading order spin-orbit coupling, Phys. Rev. D **78**, 024009 (2008).
[50] T. Damour, Coalescence of two spinning black holes: an effective one-body approach, Phys. Rev. D **64**, 124013 (2001).
[51] A. Nagar, Effective one body Hamiltonian of two spinning black-holes with next-to-next-to-leading order spin-orbit coupling, Phys. Rev. D **84**, 084028 (2011); Erratum, **88**, 089901(E) (2013).
[52] T. Damour, B. R. Iyer, and A. Nagar, Improved resummation of post-Newtonian multipolar waveforms from

circularized compact binaries, Phys. Rev. D **79**, 064004 (2009).
[53] L. Baiotti, T. Damour, B. Giacomazzo, A. Nagar, and L. Rezzolla, Analytic modelling of tidal effects in the relativistic inspiral of binary neutron stars, Phys. Rev. Lett. **105**, 261101 (2010).
[54] L. Blanchet, Gravitational radiation from post-Newtonian sources and inspiralling compact binaries, Living Rev. Relativity **9**, 4 (2006).
[55] E. E. Flanagan and S. A. Hughes, The Basics of gravitational wave theory, New J. Phys. **7**, 204 (2005).
[56] J. Centrella, J. G. Baker, B. J. Kelly, and J. R. van Meter, Black-hole binaries, gravitational waves, and numerical relativity, Rev. Mod. Phys. **82**, 3069 (2010).
[57] P. Ajith *et al.*, A template bank for gravitational waveforms from coalescing binary black holes. I. Non-spinning binaries, Phys. Rev. D **77**, 104017 (2008); Erratum, **79**, 129901(E) (2009).
[58] A. Buonanno and T. Damour, Transition from inspiral to plunge in binary black hole coalescences, Phys. Rev. D **62**, 064015 (2000).
[59] T. Delsate, D. Hilditch, and H. Witek, Initial value formulation of dynamical Chern-Simons gravity, Phys. Rev. D **91**, 024027 (2015).
[60] A. Pai, S. Dhurandhar, and S. Bose, A data analysis strategy for detecting gravitational wave signals from inspiraling compact binaries with a network of laser interferometric detectors, Phys. Rev. D **64**, 042004 (2001).
[61] S. Bose, Search templates for stochastic gravitational-wave backgrounds, Phys. Rev. D **71**, 082001 (2005).
[62] F. Pretorius, Evolution of binary black hole spacetimes, Phys. Rev. Lett. **95**, 121101 (2005).
[63] K. G. Arun, B. R. Iyer, M. S. S. Qusailah, and B. S. Sathyaprakash, Testing post-Newtonian theory with gravitational wave observations, Classical Quantum Gravity **23**, L37 (2006).
[64] P. Kanti and R. A. Konoplya, Quasi-normal modes of brane-localised standard model fields, Phys. Rev. D **73**, 044002 (2006).
[65] R. A. Konoplya and A. Zhidenko, Quasinormal modes of black holes: From astrophysics to string theory, Rev. Mod. Phys. **83**, 793 (2011).
[66] B. Toshmatov, Z. Stuchlik, J. Schee, and B. Ahmedov, Quasinormal frequencies of black hole in the braneworld, Phys. Rev. D **93**, 124017 (2016).
[67] D. Andriot and G. Lucena Gmez, Signatures of extra dimensions in gravitational waves, J. Cosmol. Astropart. Phys. 06 (2017) 048.
[68] S. S. Seahra, C. Clarkson, and R. Maartens, Detecting extra dimensions with gravity wave spectroscopy: The black string brane-world, Phys. Rev. Lett. **94**, 121302 (2005).
[69] C. Clarkson and R. Maartens, Gravity-wave detectors as probes of extra dimensions, Gen. Relativ. Gravit. **37**, 1681 (2005); Int. J. Mod. Phys. D **14**, 2347(E) (2005).
[70] S. S. Seahra and C. Clarkson, Gravitational waves in the black string braneworld, Classical Quantum Gravity **26**, 245004 (2009).
[71] C. Clarkson and S. S. Seahra, A gravitational wave window on extra dimensions, Classical Quantum Gravity **24**, F33 (2007).
[72] C. Clarkson and S. S. Seahra, Braneworld resonances, Classical Quantum Gravity **22**, 3653 (2005).
[73] S. S. Seahra, Gravitational waves from braneworld black holes, Lect. Notes Phys. **769**, 347 (2009).
[74] H. Witek, Numerical relativity in higher-dimensional space-times, Int. J. Mod. Phys. A **28**, 1340017 (2013).
[75] T. Shiromizu, K.-i. Maeda, and M. Sasaki, The Einstein equation on the 3-brane world, Phys. Rev. D **62**, 024012 (2000).
[76] S. Chakraborty and S. SenGupta, Spherically symmetric brane spacetime with bulk $f(\mathcal{R})$ gravity, Eur. Phys. J. C **75**, 11 (2015).
[77] S. Chakraborty and S. SenGupta, Effective gravitational field equations on m-brane embedded in n-dimensional bulk of Einstein and $f(\mathcal{R})$ gravity, Eur. Phys. J. C **75**, 538 (2015).
[78] S. Chakraborty and S. SenGupta, Spherically symmetric brane in a bulk of f(R) and Gauss-Bonnet gravity, Classical Quantum Gravity **33**, 225001 (2016).
[79] T. Padmanabhan, *Gravitation: Foundations and Frontiers* (Cambridge University Press, Cambridge, England, 2010).
[80] E. Poisson, *A Relativist's Toolkit: The Mathematics of Black-Hole Mechanics* (Cambridge University Press, Cambridge, England, 2007).
[81] R. Maartens, Geometry and dynamics of the brane world, in *Spanish Relativity Meeting on Reference Frames and Gravitomagnetism (EREs2000), Valladolid, Spain, September 6-9*, 2000.
[82] N. Dadhich, R. Maartens, P. Papadopoulos, and V. Rezania, Black holes on the brane, Phys. Lett. B **487**, 1 (2000).
[83] T. Harko and M. Mak, Vacuum solutions of the gravitational field equations in the brane world model, Phys. Rev. D **69**, 064020 (2004).
[84] R. Maartens and K. Koyama, Brane-world gravity, Living Rev. Relativity **13**, 5 (2010).
[85] S. Bhattacharyya and S. Shankaranarayanan, Quasinormal modes as a distinguisher between general relativity and f(R) gravity, Phys. Rev. D **96**, 064044 (2017).
[86] G. Pratten, Covariant perturbations of f(R) black holes: The Weyl terms, Classical Quantum Gravity **32**, 165018 (2015).
[87] A. Chamblin, H. S. Reall, H.-a. Shinkai, and T. Shiromizu, Charged brane world black holes, Phys. Rev. D **63**, 064015 (2001).
[88] N. Dadhich and S. G. Ghosh, Gravitational collapse of null fluid on the brane, Phys. Lett. B **518**, 1 (2001).
[89] C. D. Hoyle, D. J. Kapner, B. R. Heckel, E. G. Adelberger, J. H. Gundlach, U. Schmidt, and H. E. Swanson, Sub-millimeter tests of the gravitational inverse-square law, Phys. Rev. D **70**, 042004 (2004).
[90] J. C. Long, H. W. Chan, A. B. Churnside, E. A. Gulbis, M. C. M. Varney, and J. C. Price, Upper limits to submillimeter-range forces from extra space-time dimensions, Nature (London) **421**, 922 (2003).
[91] S. J. Smullin, A. A. Geraci, D. M. Weld, J. Chiaverini, S. P. Holmes, and A. Kapitulnik, New constraints on Yukawa-type deviations from Newtonian gravity at 20 microns, Phys. Rev. D **72**, 122001 (2005); Erratum, **72**, 129901(E) (2005).

[92] R. Gregory, Black string instabilities in Anti-de Sitter space, Classical Quantum Gravity **17**, L125 (2000).
[93] R. Gregory, The Gregory-Laflamme instability, in *Black holes in higher dimensions*, edited by G. T. Horowitz (Cambridge University Press, Cambridge, England, 2011) pp 29–43.
[94] L. Lehner and F. Pretorius, Final state of Gregory-Laflamme Instability, arXiv:1106.5184.
[95] V. P. Frolov and A. A. Shoom, Gregory-Laflamme instability of 5D electrically charged black strings, Phys. Rev. D **79**, 104002 (2009).
[96] R. A. Konoplya, K. Murata, J. Soda, and A. Zhidenko, Looking at the Gregory-Laflamme instability through quasi-normal modes, Phys. Rev. D **78**, 084012 (2008).
[97] E. W. Leaver, An analytic representation for the quasi normal modes of Kerr black holes, Proc. R. Soc. A **402**, 285 (1985).
[98] S. Chandrasekhar, *The mathematical theory of black holes* (Clarendon Press, Oxford, England, 1985) p. 646.
[99] H.-P. Nollert, Topical Review: Quasinormal modes: the characteristic 'sound' of black holes and neutron stars, Classical Quantum Gravity **16**, R159 (1999).
[100] K. D. Kokkotas and B. G. Schmidt, Quasinormal modes of stars and black holes, Living Rev. Relativity **2**, 2 (1999).
[101] P. Pani, Advanced methods in black-hole perturbation theory, Int. J. Mod. Phys. A **28**, 1340018 (2013).
[102] V. Cardoso, S. Chakrabarti, P. Pani, E. Berti, and L. Gualtieri, Floating and sinking: The Imprint of massive scalars around rotating black holes, Phys. Rev. Lett. **107**, 241101 (2011).
[103] J. G. Rosa and S. R. Dolan, Massive vector fields on the Schwarzschild spacetime: Quasi-normal modes and bound states, Phys. Rev. D **85**, 044043 (2012).
[104] R. A. Konoplya and A. Zhidenko, Stability of higher dimensional Reissner-Nordstrom-anti-de Sitter black holes, Phys. Rev. D **78**, 104017 (2008).
[105] R. A. Konoplya and A. Zhidenko, Stability and quasinormal modes of the massive scalar field around Kerr black holes, Phys. Rev. D **73**, 124040 (2006).